

Quantum Spontaneous Stochasticity

Gregory L. Eyink^{1,2} and Theodore D. Drivas¹

¹*Department of Applied Mathematics & Statistics,*

The Johns Hopkins University, Baltimore, MD, USA and

²*Department of Physics & Astronomy, The Johns Hopkins University, Baltimore, MD, USA*

(Dated: November 6, 2018)

It is commonly believed that the quantum wave-function of a very massive particle with small initial uncertainties in both position and velocity (consistent with the uncertainty relation) will spread very slowly, so that the limiting dynamics is classical Newtonian and, in particular, deterministic. This argument assumes, however, that the classical motions for given initial data must be unique. It was discovered about two decades ago in the field of fluid turbulence that non-uniqueness due to “roughness” of the (non-random) advecting velocity field may lead to stochastic motion of classical particles. Vanishingly small random perturbations are explosively magnified by turbulent Richardson diffusion in a “nearly rough” velocity field, so that motion remains stochastic as the noise disappears. This *classical spontaneous stochasticity* effect has great importance for magnetic reconnection and dynamo in astrophysics, for geophysical mixing problems, and for everyday manifestations of fluid turbulence. Simple analogies between stochastic particle motion in turbulence and quantum evolution (Wiener vs. Feynman path-integrals, Fokker-Planck vs. Schrödinger equations) suggest that there should also be *quantum spontaneous stochasticity* (QSS) driven by quantum fluctuations. We verify this idea for 1D models of a quantum particle in a repulsive potential which is “nearly rough”, with $V(x) \sim -C|x|^{1+\alpha}$ at distances $|x| \gg \ell$ for some physical UV cut-off ℓ , and for an initial Gaussian minimum-uncertainty wave-packet centered at 0. We first consider the WKB limit with $\hbar/m \rightarrow 0$, then position-spread $\sigma \rightarrow 0$. As in critical lattice systems, we show that the “infrared” limit of time $t \rightarrow \infty$ is equivalent to the “continuum” limit $\ell, \sigma \rightarrow 0$, with $\mu = \ell/\sigma$ fixed. The corresponding scaling limit of the position density is non-deterministic, with equal probabilities of the particle following either of two, non-unique classical solutions and with super-ballistic, Richardson-like spreading of the wave-packet. The splitting of the wave-packet into two peaks occurs in a very short time $t \sim \tau_c(\mu)(\ell^{1+\alpha}/C)^{1/2}$ for small ℓ . We derive the asymptotics of $\tau_c(\mu)$ for small and large μ . We also consider the scattering off the rough potential of minimum-uncertainty wave-packets with non-vanishing expectations $\langle x \rangle$, $\langle p \rangle$ and find that QSS occurs here too for careful fine-tuning of $\langle x \rangle$, $\langle p \rangle$, σ , ℓ . Beyond WKB, we also consider other semi-classical limits by a numerical solution of the Schrödinger equation, where we observe QSS both in position-space and in momentum-space. Although the wave-function remains split into two widely separated branches in the classical limit, rapid phase oscillations within each branch prevent any coherent superposition. Thus, indeterminism persists in the classical limit for rough potentials, but not quantum entanglement. These are unambiguous predictions of quantum mechanics which should be observable in laboratory experiments. We consider possible realizations by AMO, ultra-cold neutrons, and optical analogue experiments. We also briefly contrast QSS with Anderson localization.

I. INTRODUCTION

The determinism of Newtonian particle dynamics is generally taken for granted. However, the uniqueness of solutions of classical initial-value problems for ordinary differential equations (ODE’s) requires mathematical assumptions on smoothness of the velocity vector field, and there are simple counterexamples in every textbook on ODE’s when these assumptions are not satisfied (e.g. see [1], section II.5.) Such examples have engendered philosophical ruminations on acausality in classical dynamics [2]. This subject entered the realm of physics in the fundamental work of Bernard, Gawędzki and Kupiainen on particle advection in turbulent fluid flow [3], which predicted that Lagrangian particle trajectories must become non-unique and indeterministic for an exactly prescribed fluid velocity field and an exactly prescribed initial particle location, as a consequence of the “roughness” associated to a Kolmogorov energy spectrum. Those authors pointed out that stochasticity in solutions of determinis-

tic ODE’s should occur in the situation physically realized by fluid turbulence with “roughness” of the velocity field only over a finite inertial-range of scales—and thus smooth velocity fields at sufficiently small scales—when coupled with vanishingly small random perturbations to fluid trajectories. This phenomenon was later dubbed *spontaneous stochasticity* [4]. It is, in retrospect, a direct consequence of the pioneering 1926 work of L. F. Richardson on turbulent particle dispersion [5], but long unappreciated. This phenomenon has profound consequences in astrophysics, for example, where spontaneous stochasticity of plasma fluid motions breaks the ideal constraint of magnetic flux-freezing even in the limit of infinite conductivity and allows magnetic reconnection to be fast [6–9]. Analogous breaking of the Kelvin-Helmholtz theorems on vortex-line motions occurs in hydrodynamic turbulence [10], with consequences for turbulent mixing of vorticity in geophysical and engineering flows.

The empirical verification of spontaneous stochasticity effects in fluid and plasma turbulence currently rests

upon numerical simulations of the Navier-Stokes and magnetohydrodynamics equations [9, 11, 12]. The phenomenon has not yet been seen in controlled laboratory experiments of turbulent flows [13], presumably because of the technical difficulties in tracking advected particle pairs that start sufficiently close together. The best prospect for fluid turbulence experiments is to make a bigger flow apparatus with a larger Reynolds number. In this way, particles even at relatively large initial separations have sufficient time within the inertial-range to exhibit the effects. An alternative idea that we explore here is instead to go smaller and to search for analogous effects in the quantum world. There is in fact intrinsic interest in the question of how a quantum system will behave whose corresponding classical dynamics is (nearly) non-unique. As we shall see, this situation leads to quantum randomness surviving in the classical limit where one normally expects determinism to prevail. Before demonstrating this, we first review briefly the phenomenon of classical spontaneous stochasticity.

II. BACKGROUND

The results of Richardson's theory of particle dispersion in turbulent flow can be most easily understood from a toy model for the growth of separation r between a pair of particles advected by the flow:

$$dr/dt = C(\varepsilon r)^{1/3}, \quad (1)$$

where the righthand side represents the relative velocity $\delta u(r)$ of the particles at separation r . The scaling with exponent $1/3$ is consistent with the statistical theory of Kolmogorov [14]. Solving by separation of variables gives the exact solution

$$r(t) = \left(r_0^{2/3} + \frac{2}{3} C \varepsilon^{1/3} t \right)^{3/2}$$

which exhibits the Richardson scaling $r^2(t) \propto \varepsilon t^3$ [5] for $t \gg r_0^{2/3}/\varepsilon^{1/3}$. More surprisingly, however,

$$r(t) \rightarrow \left(\frac{2}{3} C \varepsilon^{1/3} t \right)^{3/2} > 0$$

as $r_0 \rightarrow 0$. Thus, two particles at identically the same initial point, with $r_0 = 0$, end up a finite distance apart at any positive time! One's natural expectation would be instead that $r(t) \equiv 0$ and that the two particles would move together for all time. In fact, these are just two examples of infinitely-many solutions of the initial value problem for equation (1) with $r_0 = 0$. The most general solution has, for any waiting time $\tau \in [0, \infty]$, $r(t) = 0$ for $t \leq \tau$ and then $r(t) = \left(\frac{2}{3} C \varepsilon^{1/3} (t - \tau) \right)^{3/2}$ for $t > \tau$.

The above toy problem is the standard example of general theorems on the non-uniqueness of solutions of the initial-value problem for an ODE:

$$d\mathbf{x}/dt = \mathbf{u}(\mathbf{x}, t), \quad \mathbf{x}(t_0) = \mathbf{x}_0. \quad (2)$$

If the advecting velocity field satisfies a spatial Hölder continuity condition

$$|\mathbf{u}(\mathbf{x} + \mathbf{r}) - \mathbf{u}(\mathbf{x})| \leq C|\mathbf{r}|^\alpha \quad (3)$$

for $\alpha = 1$ (a so-called Lipschitz condition) then solutions are unique, but examples like the previous one with $\alpha = 1/3$ show that solutions need not be unique for $0 < \alpha < 1$ [1]. The latter situation is the expected one for turbulence. At the level of individual flow realizations, it was shown by Onsager [15, 16] that the observed energy dissipation anomaly for turbulent flow requires that in the limit of infinite Reynolds number the fluid velocity field must have a Hölder exponent $\alpha \leq 1/3$ and, in particular, \mathbf{u} cannot remain space-differentiable as $Re \rightarrow \infty$.

Real fluid turbulence has, of course, a finite Reynolds number albeit possibly very large. Thus, the velocity field is ultimately smooth and satisfies a bound of the form (3) with $\alpha = 1$ for $|\mathbf{r}| < \eta$, a small length-scale set by viscosity ν . For example, in the Kolmogorov theory, $\eta = \nu^{3/4} \varepsilon^{-1/4}$. Thus, particle trajectories are unique. However, it was realized in [3] that the non-uniqueness resurfaces for the fluid trajectories with small random perturbations to the dynamics or to the initial data. That paper considered the specific problem of stochastic particle trajectories satisfying a Langevin equation

$$d\tilde{\mathbf{x}}/dt = \mathbf{u}_\nu(\tilde{\mathbf{x}}, t) + \sqrt{2\kappa} \tilde{\boldsymbol{\eta}}(t), \quad \tilde{\mathbf{x}}(t_0) = \mathbf{x}_0 + \rho \tilde{\boldsymbol{\xi}} \quad (4)$$

with $\mathbf{u}_\nu(\mathbf{x}, t)$ the turbulent fluid velocity field, with $\tilde{\boldsymbol{\eta}}(t)$ a vector white-noise, and with $\tilde{\boldsymbol{\xi}}$ any random vector with zero mean and finite variance. The subscript ν stands for the (kinematic) viscosity of the fluid, which is a finite, positive value. This stochastic evolution is relevant to the problem of an advected passive scalar θ (e.g. temperature or dye concentration) satisfying

$$\partial_t \theta(\mathbf{x}, t) + \mathbf{u}_\nu(\mathbf{x}, t) \cdot \nabla \theta(\mathbf{x}, t) = \kappa \Delta \theta(\mathbf{x}, t). \quad (5)$$

In fact, if $p_\nu(\mathbf{x}', t' | \mathbf{x}, t)$ is the transition probability density for the stochastic evolution, then

$$\theta(\mathbf{x}, t) = \int d^d x_0 \theta(\mathbf{x}_0, t_0) p_\nu(\mathbf{x}_0, t_0 | \mathbf{x}, t), \quad t_0 < t.$$

It is convenient to express the transition probability by a Wiener path-integral [3, 11, 17]

$$p_\nu(\mathbf{x}, t | \mathbf{x}_0, t_0) = \int_{\boldsymbol{\xi}(t_0)=\mathbf{x}_0} \mathcal{D}\boldsymbol{\xi} \delta^d(\mathbf{x} - \boldsymbol{\xi}(t)) \times \exp \left(-\frac{1}{4\kappa} \int_{t_0}^t ds |\dot{\boldsymbol{\xi}}(s) - \mathbf{u}_\nu(\boldsymbol{\xi}(s), s)|^2 \right) \quad (6)$$

If the velocity field \mathbf{u} remains smooth (i.e. if the viscosity ν is held fixed), then a steepest descent argument on the path-integral shows that as $\kappa \rightarrow 0$

$$p_\nu(\mathbf{x}, t | \mathbf{x}_0, t_0) \rightarrow \delta^d(\mathbf{x} - \mathbf{x}_t(\mathbf{x}_0))$$

where $\mathbf{x}_t(\mathbf{x}_0)$ is the unique solution of the initial-value problem (2). However, if the turbulent velocity field becomes only Hölder continuous, as when taking the limit

$\nu, \kappa \rightarrow 0$ together, then it was shown in [3] that a non-trivial limit $p_*(\mathbf{x}, t|\mathbf{x}_0, t_0)$ may result. Thus, the particle trajectories remain random as the external noise is removed and the deterministic problem (2) is recovered.

There is a close analogy of this “spontaneous stochasticity” with the zero-temperature phase transition in the 1D Ising model [18]. We may write the 1D Ising model in finite-volume $[-N, \dots, N]$ as a Gibbs distribution $P_N[\sigma] = \frac{1}{Z} \exp\left(-\frac{1}{k_B T} H[\sigma]\right)$ for Hamiltonian

$$H[\sigma] = \frac{J}{2} \sum_{\substack{i=-N \\ \sigma_{-N}=+1}}^N (\sigma_i - \sigma_{i+1})^2$$

with boundary condition $\sigma_{-N} = +1$ and free boundary condition on σ_N . To emphasize the analogy with the path-integral (6), we have rewritten the Ising model Hamiltonian as a sum of squares and imposed a boundary condition only at the left endpoint. In the zero-temperature limit at fixed N ,

$$P_N[\sigma] \rightarrow \prod_{i=-N}^N \delta_{\sigma_i, +1} \text{ as } T \rightarrow 0,$$

the unique ground-state with $\sigma_{-N} = +1$. On the other hand, if the infinite-volume limit $N \rightarrow \infty$ is taken first before taking the zero-temperature limit, then

$$P_\infty[\sigma] \rightarrow \frac{1}{2} \prod_i \delta_{\sigma_i, +1} + \frac{1}{2} \prod_i \delta_{\sigma_i, -1} \text{ as } T \rightarrow 0,$$

the symmetric mixture of infinite-volume ground-states. This is the well-known zero-temperature phase transition in the 1D Ising model. The phenomenon discovered in [3] for non-smooth dynamical systems is exactly analogous, with the viscosity ν corresponding to N , the noise κ to temperature T , and the non-unique solutions of the initial-value problem (2) corresponding to the non-unique ground states of the infinite-volume Ising model.

The results of [3] were obtained for a soluble turbulence model, the Kraichnan model [19, 20], in which the fluid velocity field is replaced by a “synthetic turbulence” consisting of a Gaussian random field which is delta-correlated in time. The results on spontaneous stochasticity hold with probability one for every realization of the Gaussian velocity field. These results in the Kraichnan model have been confirmed and further elaborated in many subsequent works [4, 21–25]. The current evidence of these effects in fluid turbulence described by the Navier-Stokes equations consists of numerical studies of mean-square pair-dispersion $\langle r^2(t) \rangle$, where the average is over the initial space position \mathbf{x} of the pair in a single flow realization. These studies confirm the Richardson prediction $\langle r^2(t) \rangle \propto \varepsilon t^3$ and, even more importantly, provide evidence that the pair-dispersion for particles evolving under the stochastic evolution (4) becomes independent of κ after a short time of order $(\kappa/\varepsilon)^{1/2}$ [11], or, similarly, that the pair-dispersion for particles evolving under the deterministic equation (1) becomes independent

of the initial separation r_0 after a time of order $r_0^{2/3}/\varepsilon^{1/3}$ [12]. Indirect evidence for spontaneous stochasticity is also afforded by experimental observation of anomalous dissipation of passive scalars in fluid turbulent flows [26].

There is a close similarity of the path-integral (6) for the transition probability of the stochastic advection problem and the Feynman path-integral for the transition amplitude in quantum theory [27]. Consider a non-relativistic quantum-mechanical particle of mass m and electric charge q moving in an electric field $\mathbf{E} = -\nabla\Phi - (1/c)\partial_t\mathbf{A}$ and magnetic field $\mathbf{B} = \nabla\times\mathbf{A}$ governed by the Schrödinger equation

$$i\hbar\partial_t\psi = \frac{1}{2m} \left(-i\hbar\nabla - \frac{q}{c}\mathbf{A}\right)^2 \psi + q\Phi\psi.$$

Then Feynman represented the transition amplitudes by the formula

$$\langle \mathbf{x}, t | \mathbf{x}_0, 0 \rangle = \int_{\mathbf{x}(0)=\mathbf{x}_0}^{\mathbf{x}(t)=\mathbf{x}} \mathcal{D}\mathbf{x} \exp\left(\frac{i}{\hbar} \int_0^t ds L(\mathbf{x}(s), \dot{\mathbf{x}}(s), s)\right),$$

where the classical Lagrangian is

$$L(\mathbf{x}, \dot{\mathbf{x}}, t) = \frac{1}{2}m|\dot{\mathbf{x}}|^2 + \frac{q}{c}\mathbf{A}(\mathbf{x}, t) \cdot \dot{\mathbf{x}} - q\Phi(\mathbf{x}, t).$$

Not only is Feynman’s formula analogous to (6), but it can be used to derive (6) ([11], Appendix). This close relation naturally raises the question whether *quantum-spontaneous stochasticity* effects can arise in the classical limit, given formally by $\hbar \rightarrow 0$. When \mathbf{E}, \mathbf{B} are Lipschitz, then the classical equations of motion

$$m\ddot{\mathbf{x}} = q \left[\mathbf{E}(\mathbf{x}, t) + \frac{1}{c} \dot{\mathbf{x}} \times \mathbf{B}(\mathbf{x}, t) \right]$$

have unique solutions and the stationary phase argument of Feynman [27] yields classical dynamics for $\hbar \rightarrow 0$. However, if the electromagnetic fields are non-Lipschitz, then quantum randomness could possibly persist in the classical limit.

Similar questions have been raised previously in the literature. An interesting recent mathematical study [28, 29] has considered the classical limit for the simplest 1D Hamiltonian system whose classical solutions are non-unique. See eqs. (7)-(9) below. In this example a power-law potential leads to a force field which is Hölder continuous with an exponent $\alpha < 1$. It was proved in [28] that the Wigner function for the quantum particle converges in the formal classical limit $\hbar \rightarrow 0$ to a non-trivial probability measure, so that indeterminacy persists in the limit. This mathematical result assumes, however, an exact power-law potential down to zero-length scale, i.e. to the Planck length and below! The physical validity of the nonrelativistic Schrödinger equation with a classical potential will break down well before this scale, e.g. quantum electrodynamic effects such as particle pair-production will become relevant at the Compton wavelength h/mc . In any case, an exact power-law down to

zero length-scales should not be necessary to obtain such effects, just as [3] showed for the problem of turbulent advection. The main aim of our work will be to introduce physical short-distance cut-offs into the model of [28] and to show that quantum spontaneous stochasticity effects exist in experimentally accessible regimes. The need for such a short-distance cut-off was realized in previous work of Blümel [30], who studied a related phenomenon of “quantum ray-splitting” in discontinuous step-potentials (see also [31, 32]). In this case also, quantum randomness persists in the classical limit of vanishing de Broglie wavelength λ as the short-distance cut-off ℓ is taken simultaneously to zero. Such step-potentials lead, however, to very singular delta-function forces. The innovation of our work will be to show that such effects can occur with much smoother force fields which, even as the cut-off ℓ is removed, remain bounded and continuous.

III. MODELS

Just as in [28], we consider the model of a single particle moving in a repulsive, scale-invariant cusp (or conic) potential energy field

$$V(x) = -\frac{C}{1+\alpha}|x|^{1+\alpha}, \quad 0 < \alpha < 1. \quad (7)$$

In fact, we take V to be the potential energy per mass m of the particle, so the constant $C > 0$ absorbs a factor of $1/m$. The classical dynamics is thus given by the ODE

$$\dot{x} = v, \quad \dot{v} = C|x|^\alpha \text{sign}(x), \quad (8)$$

which are Hamiltonian with $H = \frac{1}{2}v^2 + V(x)$. The flow vector field $\mathbf{U}(x, v) = (v, C|x|^\alpha \text{sign}(x))$ is infinitely differentiable except at points of the form $(x, v) = (0, v_0)$, where it is only Hölder continuous with exponent α . In particular,

$$|\mathbf{U}(r, 0) - \mathbf{U}(0, 0)| = C|r|^\alpha,$$

at point $(x, v) = (0, 0)$. It is not hard to show that the solutions of the initial-value problem are unique at all starting points except those that lead to solutions passing through $(x, v) = (0, 0)$, where there are infinitely many solutions. The two extremal solutions starting at $(x_0, v_0) = (0, 0)$ for initial time $t_0 = 0$ (which reach the farthest distance at each later time t) are

$$x_\pm(t) = \pm \left[\frac{1}{2}(1-\alpha) \left(\frac{2C}{1+\alpha} \right)^{1/2} t \right]^{2/(1-\alpha)}. \quad (9)$$

There are infinitely many other solutions for this same initial condition in which the particle waits at $x = 0$ for a time $\tau \in [0, \infty]$, before moving off in the same manner.

The general solution of the initial-value problem for (8) can be obtained by quadrature using energy conservation,

which reduces the system of two equations to a single first-order ODE for $|x(t)|$:

$$\frac{d}{dt}|x| = \pm \sqrt{\frac{2C}{1+\alpha}|x|^{1+\alpha} + H_0}, \quad x(t_0) = x_0 \quad (10)$$

with \pm representing $\text{sign}(x \cdot v)$ and $H_0 = \frac{1}{2}v_0^2 + V(x_0)$. For any $H_0 < 0$, one can write $H_0 = -\frac{C}{1+\alpha}|\bar{x}_0|^{1+\alpha}$ where \bar{x}_0 satisfying $|\bar{x}_0| < |x_0|$ is the position of a particle instantaneously at rest with the same energy. Separating variables yields [33] an implicit solution in terms of hypergeometric functions ([34], Ch.15; [35], Ch.II):

$$\begin{aligned} & |x|^{(1-\alpha)/2} {}_2F_1 \left(\frac{1}{2}, -\frac{(1-\alpha)}{2(1+\alpha)}; \frac{1+3\alpha}{2(1+\alpha)}; + \left| \frac{\bar{x}_0}{x} \right|^{1+\alpha} \right) \\ & - |x_0|^{(1-\alpha)/2} {}_2F_1 \left(\frac{1}{2}, -\frac{(1-\alpha)}{2(1+\alpha)}; \frac{1+3\alpha}{2(1+\alpha)}; + \left| \frac{\bar{x}_0}{x_0} \right|^{1+\alpha} \right) \\ & = \pm \frac{1}{2}(1-\alpha) \left(\frac{2C}{1+\alpha} \right)^{1/2} (t - t_0). \end{aligned} \quad (11)$$

If $\text{sign}(x_0 \cdot v_0) < 0$, then the $-$ sign holds initially and $|x|$ decreases to $|\bar{x}_0|$, whereupon the velocity reverses direction, $|x|$ increases and the $+$ sign holds. For $H_0 > 0$ there is a similar formula obtained by writing $H_0 = \frac{C}{1+\alpha}|\bar{x}_0|^{1+\alpha}$, but with the $+$ sign in the main argument of the hypergeometric function changed to a $-$ sign. In this case, v never changes sign, but $|x|$ may pass through 0 with a corresponding change of overall sign on the righthand side from $-$ to $+$. It is easy to see from the exact solution (11) that, for all choices of initial conditions (x_0, v_0) , the ratio $x(t)/x_\pm(t) \rightarrow 1$ as $t \rightarrow \infty$ for one choice of \pm . This “forgetting” of the initial data is the essence of spontaneous stochasticity.

A physically realizable potential will however exhibit a power-law scaling as in (7) only over a limited range of x -values, with an “inner” or short-distance cutoff ℓ and an “outer” or large-distance cut-off L . We shall not introduce an explicit cutoff L at large-distances, but we can use our results with $L = \infty$ to estimate the practical effects of such a cut-off. We introduce two concrete models with a short-distance cut-off ℓ . The first is a globally analytic potential given by a confluent hypergeometric or Kummer function ([34], Ch.13; [35], Ch.VI; [36], Ch.IV):

$$\begin{aligned} V_\ell(x) = & -C\ell^{1+\alpha} \frac{2^{(1+\alpha)/2} \Gamma((2+\alpha)/2)}{(1+\alpha)\sqrt{\pi}} \\ & \times {}_1F_1 \left(-\frac{1}{2}(1+\alpha), \frac{1}{2}; -\frac{x^2}{2\ell^2} \right) \end{aligned} \quad (12)$$

We shall refer to this as the “Kummer potential”. It can be obtained by convolving the power-law potential in (7) with a Gaussian smoothing kernel $\exp(-x^2/2\ell^2)/\sqrt{2\pi\ell^2}$, and thus becomes indistinguishable from the power-law for $|x| \gg \ell$. The second model potential is chosen to coincide exactly with the power-law for $|x| \geq \ell$ but is only piecewise smooth with continuous first-derivatives

at $|x| = \ell$, given by the elementary formulas:

$$V_\ell(x) = \begin{cases} -\frac{1}{2}C\ell^{1+\alpha} \left(\frac{1-\alpha}{1+\alpha} + \frac{x^2}{\ell^2} \right), & |x| < \ell \\ -\frac{C}{1+\alpha}|x|^{1+\alpha}, & |x| \geq \ell \end{cases}. \quad (13)$$

We shall refer to this as the ‘‘first-order spliced potential’’. It has less generic behavior because of its lower degree of spatial smoothness but it is more tractable for analytic calculations.

The main problem that we shall consider is the quantum evolution in these potentials of an initial minimum-uncertainty Gaussian wave-packet

$$\psi_0(x) = \frac{1}{(2\pi\sigma^2)^{1/4}} \exp\left(-\frac{(x - \langle x \rangle)^2}{4\sigma^2} + \frac{1}{\hbar}i\langle p \rangle x\right) \quad (14)$$

with mean $\langle x \rangle$ and uncertainty σ in position-space and mean $\langle p \rangle$ and uncertainty $\hbar/2\sigma$ in momentum-space. There is a clear analogy with the problem of turbulent transport, which we make explicit in the table below:

Turbulence-Quantum Analogy	
Turbulent Advection	Quantum Mechanics
Fokker-Planck equation	Schrödinger equation
$\partial_t p = \kappa \Delta p - \nabla \cdot (\mathbf{u}p)$	$i\partial_t \psi = \frac{\hbar}{2m} \Delta \psi + \frac{V}{\hbar} \psi$,
Velocity integral length L	Outer length L of potential
Dissipation length η	Inner length ℓ of potential
Scalar diffusivity κ	Quantum of circulation \hbar/m
Position uncertainty ρ	Wavepacket spread σ
Reynolds number $Re = (L/\eta)^{4/3}$	Scale ratio L/ℓ of potential

Note that the Fokker-Planck equation for the probability distribution $p(\mathbf{x}, t)$ of an advected particle is the adjoint to the passive scalar equation (5). Similar analogies between high-Reynolds-number turbulence and the classical limit of Schrödinger evolution have been pointed out already some time ago (e.g. [37], section 6), but little pursued up until now.

IV. WKB ANALYSIS

We shall first analyze our model problem in the limit where the de Broglie wavelength $\lambda = \hbar/mv$ of the particle is much smaller than the inner length ℓ of the potential. This is the usual semi-classical or WKB limit. In the turbulence-quantum analogy sketched above, this corresponds to the limit of very large Prandtl number $Pr = \nu/\kappa$. As discussed elsewhere ([11], section IV) classical spontaneous stochasticity effects are expected to be observable for Lagrangian particle dispersion in high-Prandtl number turbulent flows at sufficiently long times. This is an importance astrophysical regime appearing in the interstellar [38] and intracluster [39] media and relevant to problems of star formation [40]. It should be

stressed that the WKB limit is not necessary for quantum spontaneous stochasticity but it is probably one of the easiest regimes to study experimentally and, also, it has the conceptual advantage that the relation between the quantum and classical dynamics is transparent.

We apply the standard time-dependent WKB approximation [41–43], which corresponds to making the ansatz

$$\psi(x, t) = \exp(i\Theta(x, t)/\hbar)$$

for the solution of the Schrödinger equation, together with the asymptotic expansion

$$\Theta(x, t) = S(x, t) + (\hbar/i)S_1(x, t) + (\hbar/i)^2 S_2(x, t) + \dots$$

Dropping quadratic terms and higher, this gives

$$\psi(x, t) = \sqrt{\rho(x, t)} \exp(iS(x, t)/\hbar)$$

with $\rho(x, t) = \exp(2S_1(x, t))$, and plugging into the Schrödinger equation yields the Hamilton-Jacobi equation (or eikonal equation) for the classical action $S(x, t)$:

$$\partial_t S(x, t) + \frac{1}{2m} |\nabla S(x, t)|^2 + V(x) = 0,$$

together with the conservation (transport) equation for the position probability density $\rho(x, t)$:

$$\partial_t \rho(x, t) + \nabla \cdot (v(x, t)\rho(x, t)) = 0$$

with $v(x, t) = \nabla S(x, t)/m$ the classical velocity. These equations are most easily solved by method of characteristics, using Hamilton’s equations of motion

$$\dot{x} = p/m, \quad \dot{p} = -\nabla V(x) \quad (15)$$

with the initial conditions $x(0) = x_0$ and $p(0) = \nabla S_0(x_0)$. Calling the resulting solutions $x_t(x_0)$ and $p_t(x_0)$, it follows that $S(x_t(x_0), t) = S_t(x_0)$ with

$$S_t(x_0) = S_0(x_0) + \int_0^t ds \left[\frac{1}{2m} p_s^2(x_0) - V(x_s(x_0)) \right]. \quad (16)$$

The probability conservation equation can likewise be integrated along characteristics as

$$\rho(x_t(x_0), t) = \frac{\rho_0(x_0)}{J_t(x_0)} \quad (17)$$

where we have introduced the Jacobian

$$J_t(x_0) = \partial x_t(x_0) / \partial x_0 = x'_t(x_0).$$

To calculate the latter it is most convenient to differentiate Hamilton’s equations to obtain a set of ODE’s

$$\dot{j} = K, \quad \dot{K} = -V''(x)J \quad (18)$$

for $J_t(x_0)$ and $K_t(x_0) = p'_t(x_0)$.

We apply these standard results to our model problems. Our scaling of V corresponds to setting $m = 1$. The initial Gaussian wave-packet (14) corresponds to taking

$$S_0(x) = \langle p \rangle \cdot x, \quad \rho_0(x) = \frac{1}{\sqrt{2\pi\sigma^2}} \exp\left(-\frac{(x - \langle x \rangle)^2}{2\sigma^2}\right).$$

In that case, we have initial conditions in the ODE's

$$x(0) = x_0, \quad p(0) = \langle p \rangle, \quad J(0) = 1, \quad K(0) = 0.$$

There are no caustics for this problem, so that the WKB approximation is globally valid in time. As usual, the WKB approximation is locally valid in space when

$$\left| \lambda \frac{\partial}{\partial x} \left(\frac{p^2}{2m} \right) \right| \ll \max \left\{ \frac{p^2}{2m}, \left| \frac{\partial S}{\partial t} \right|, |V| \right\}$$

where $\lambda(x, t) = \hbar/p(x, t)$ is a local de Broglie wavelength with $p(x, t) = \partial S(x, t)/\partial x$. E.g. see [41]. This corresponds to our starting assumption $\lambda \ll \ell$ when the classical action $S(x, t)$ develops no smaller length-scales than in the potential $V(x)$. Note finally that the Schrödinger equation divided by m is

$$i \frac{\hbar}{m} \partial_t \psi = -\frac{1}{2} \left(\frac{\hbar}{m} \right)^2 \Delta \psi + V \psi \quad (19)$$

where $V/m \rightarrow V$ now represents in reality the potential energy per mass. Thus, holding V fixed, the only dependence of \hbar is through the ratio \hbar/m and one may, by varying m , study the problem formally with $m = 1$ and varying \hbar . (Of course, the dependence of V on m must be remembered in comparing results with experiment.)

A. Scaling Limit

We shall begin by studying in this and the following section the symmetrical problem with $\langle x \rangle = \langle p \rangle = 0$. We are interested here primarily in the probability density $\rho(x, t)$ for the location of the particle. Since in the WKB limit there is no dependence of $\rho(x, t)$ upon Planck's constant \hbar , it contains only dimensional parameters σ, ℓ and C , in addition to x, t . It is natural to introduce a dimensionless *scaled position*

$$\hat{x} = x/x_+(t).$$

Then simple dimensional analysis gives

$$\rho(x, t; \sigma, \ell, C) = \frac{1}{x_+(t)} \hat{\rho}(x/x_+(t), \tau; \mu)$$

where $\hat{\rho}$ is the probability density of \hat{x} and

$$\tau = t/(\ell^{1-\alpha}/C)^{1/2}, \quad \mu = \ell/\sigma.$$

This result tells us that while keeping the ratio $\mu = \ell/\sigma$ fixed, the limits $t \rightarrow \infty$ and $\ell, \sigma \rightarrow 0$ are identical. Quantum spontaneous stochasticity will be present if

$$\hat{\rho}(\hat{x}, \tau; \mu) \xrightarrow{\tau \rightarrow \infty} \frac{1}{2} \delta(\hat{x} + 1) + \frac{1}{2} \delta(\hat{x} - 1), \quad (20)$$

or, equivalently, if at fixed time t

$$\rho(x, t; \sigma, \ell, C) \rightarrow \frac{1}{2} \delta(x - x_-(t)) + \frac{1}{2} \delta(x - x_+(t))$$

in the limit $\sigma, \ell \ll (Ct^2)^{1/(1-\alpha)}$. Such a limit was obtained in [28] for the exact power-law potential. We now establish it here for the model with UV cut-off ℓ .

To prove this result, we smear $\hat{\rho}$ with a smooth test function $\varphi(\hat{x})$, giving

$$\int d\hat{x} \varphi(\hat{x}) \hat{\rho}(\hat{x}, \tau) = \int dx \varphi(x/x_+(t)) \rho(x, t).$$

Using the WKB formula (17), this can furthermore be written as

$$\int d\hat{x} \varphi(\hat{x}) \hat{\rho}(\hat{x}, \tau) = \int dx_0 \varphi(x_t(x_0)/x_+(t)) \rho_0(x_0),$$

where we used the definition $J_t = \partial x_t / \partial x_0$ to change the integration variable to x_0 . The essence of the result is now to show that

$$\lim_{t \rightarrow \infty} x_t(x_0)/x_+(t) = \pm 1, \quad (21)$$

with $\pm = \text{sign}(x_0)$. In fact, this yields a more general result than (20), for any choice of $\rho_0(x)$ which contains no delta function part $\propto \delta(x)$. In that case, we can write

$$\begin{aligned} \int d\hat{x} \varphi(\hat{x}) \hat{\rho}(\hat{x}, \tau) &= \int_{-\infty}^0 dx_0 \varphi(x_t(x_0)/x_+(t)) \rho_0(x_0) \\ &+ \int_0^{\infty} dx_0 \varphi(x_t(x_0)/x_+(t)) \rho_0(x_0), \end{aligned}$$

and apply dominated convergence to infer that

$$\lim_{\tau \rightarrow \infty} \int d\hat{x} \varphi(\hat{x}) \hat{\rho}(\hat{x}, \tau) = \varphi(-1)p_- + \varphi(1)p_+,$$

with

$$p_- = \int_{-\infty}^0 dx_0 \rho_0(x_0), \quad p_+ = \int_0^{\infty} dx_0 \rho_0(x_0).$$

This gives as a special case the result (20) for any symmetrical choice of ρ_0 with $p_- = p_+ = 1/2$.

We now demonstrate the crucial result (21) for the first-order spliced potential. Here we can develop explicit solutions for x_t and v_t . For $x_0 < \ell$ it is straightforward to show that

$$x_t(x_0) = x_0 \cosh\left(\frac{C^{1/2}t}{\ell^{(1-\alpha)/2}}\right) \quad (22)$$

when $t < t_\ell(x_0)$ with the definition

$$t_\ell(x_0) = \frac{\ell^{(1-\alpha)/2}}{C^{1/2}} \text{arccosh}(\ell/x_0),$$

at which time $x_t = \ell$. Thereafter one can use (11) to write

$$|x_t|^{(1-\alpha)/2} {}_2F_1\left(\frac{1}{2}, -\frac{(1-\alpha)}{2(1+\alpha)}; \frac{1+3\alpha}{2(1+\alpha)}; + \left| \frac{\bar{x}_0}{x_t} \right|^{1+\alpha}\right)$$

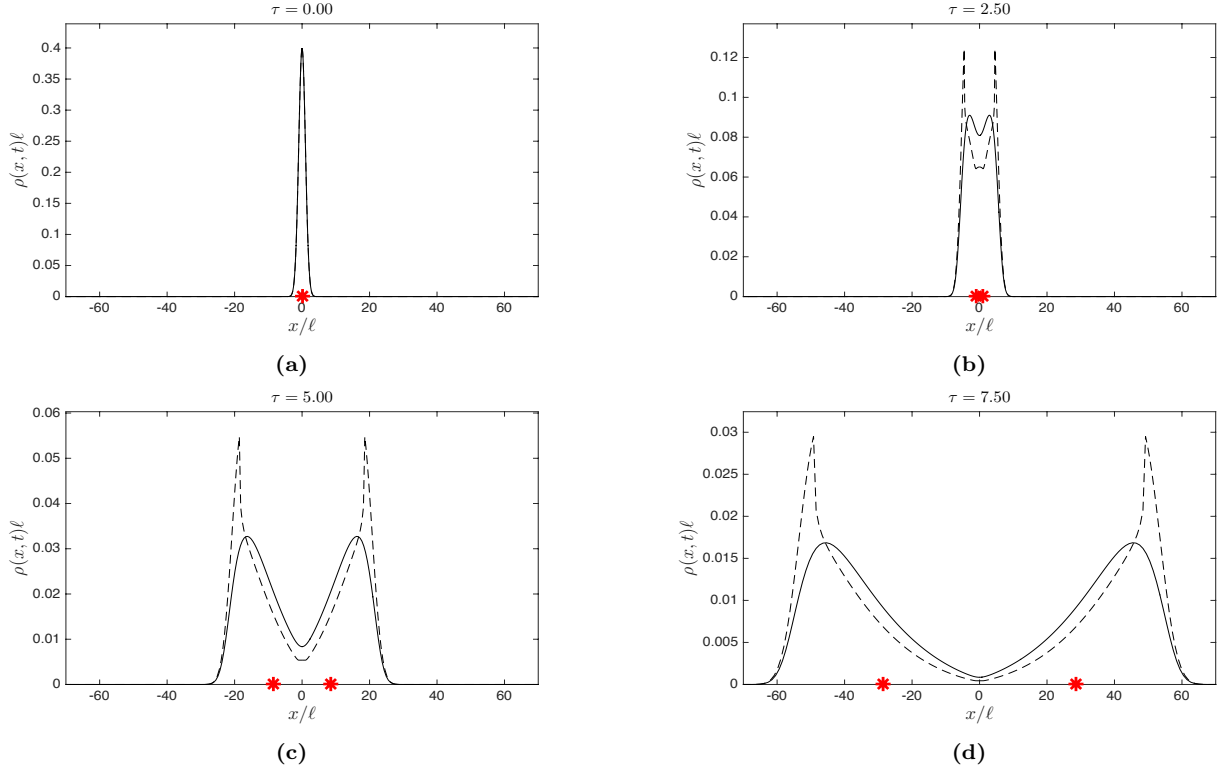


FIG. 1 WKB position-space probability densities for $\mu = 1$ and dimensionless times $\tau = 0.0, 2.5, 5.0, 7.5$. Solid is for the Kummer potential, dashed for the spliced potential, both with $\alpha = 1/3$. The two asterisks on the abscissa indicate the locations of the extremal classical solutions at the particular time of each snapshot. For movie, see [33].

$$\begin{aligned}
 & -\ell^{(1-\alpha)/2} {}_2F_1\left(\frac{1}{2}, -\frac{(1-\alpha)}{2(1+\alpha)}; \frac{1+3\alpha}{2(1+\alpha)}; +\left|\frac{\bar{x}_0}{\ell}\right|^{1+\alpha}\right) \\
 & = \frac{1}{2}(1-\alpha) \left(\frac{2C}{1+\alpha}\right)^{1/2} (t - t_\ell(x_0)). \quad (23)
 \end{aligned}$$

for $t > t_\ell(x_0)$ where it follows directly from the definition of the spliced potential (13) that

$$|\bar{x}_0|^{1+\alpha} = \ell^{1+\alpha} \left(\frac{1}{2}(1-\alpha) + \frac{1}{2}(1+\alpha) \left(\frac{x_0}{\ell}\right)^2 \right),$$

with \bar{x}_0 as an “effective initial position.” On the other hand, if $x_0 > \ell$, then the particle starts in the region where the cusp potential is exact and for all times $t > 0$ the result (11) gives

$$\begin{aligned}
 & |x_t|^{(1-\alpha)/2} {}_2F_1\left(\frac{1}{2}, -\frac{(1-\alpha)}{2(1+\alpha)}; \frac{1+3\alpha}{2(1+\alpha)}; +\left|\frac{x_0}{x_t}\right|^{1+\alpha}\right) \\
 & - |x_0|^{(1-\alpha)/2} {}_2F_1\left(\frac{1}{2}, -\frac{(1-\alpha)}{2(1+\alpha)}; \frac{1+3\alpha}{2(1+\alpha)}; +1\right) \\
 & = \frac{1}{2}(1-\alpha) \left(\frac{2C}{1+\alpha}\right)^{1/2} t. \quad (24)
 \end{aligned}$$

Here we have used the fact that $\bar{x}_0 = x_0$ in this region. To prove (21) we use these exact formulas and the fact that, for $\langle p \rangle = 0$, solutions $x_t(x_0)$ preserve the sign of x_0 . Since the righthand sides of both (23) and (24) are

asymptotic to $(x_+(t))^{(1-\alpha)/2}$ as $t \rightarrow \infty$, one gets easily that $x_t(x_0)/x_+(t) \rightarrow \text{sign}(x_0)$. This is also true for the fixed point $x_0 = 0$, with the convention that $\text{sign}(0) = 0$.

The above results should carry over qualitatively to every potential which has the power-law form (7) for some long range of x , $\ell \ll |x| \ll L$, but smoother behavior at $x \ll \ell$ preserving the repulsive character of the potential. For x_0 near 0 there will be an initial period where the classical particle position $x_t(x_0)$ moves away from the origin exponentially quickly, until the particle enters the region of power-law behavior of the potential. The particle will then move outward “explosively”, approaching one of the extremal solutions $x_\pm(t)$ at long times for every initial condition x_0 . We illustrate this with WKB results on the position probability density (PDF) for both Kummer and spliced potentials. The default values will be $\alpha = 1/3$ and $\mu = 1$ in these and all later figures, unless stated otherwise. The results were obtained by numerically integrating the ODE’s (15),(18) for logarithmically evenly spaced initial $x_0 = 10^{i/N_F}$ and integers $i = N_S N_F, \dots, N_B N_F$ with $N_F, N_S < N_B$ chosen to provide suitable resolution and then using formula (17) to evaluate the position PDF. Because of the symmetry of the problem, we could consider only $x_0 > 0$. The convergence of the results was tested by varying N_F, N_S, N_B and also by verifying that the total probability was unity to within at least a percent (and usually much closer).

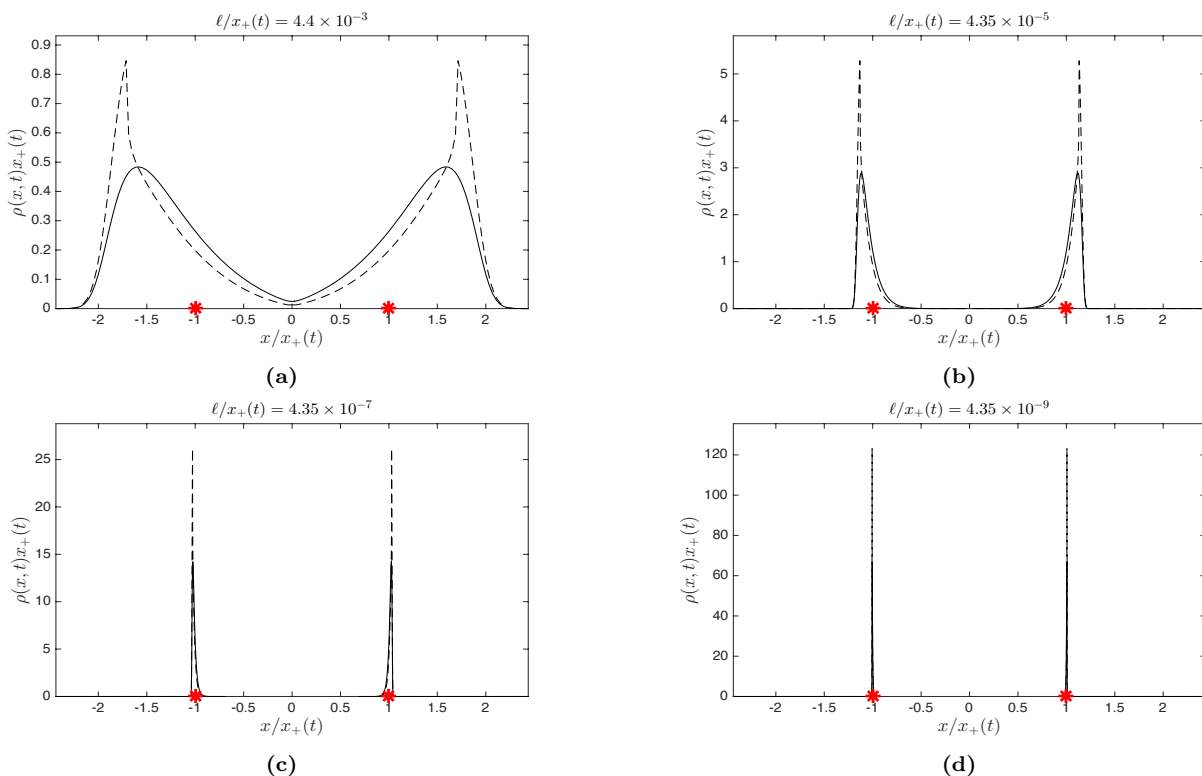


FIG. 2 WKB position-space probability densities at a fixed time t for $\mu = 1$ and $\ell/x_+(t) = 4.35 \times 10^{-3}, 10^{-5}, 10^{-7}, 10^{-9}$. Notations as in Fig. 1. For movie, see [33].

For details of the numerical methods, see [33]. Fig. 1 shows the time evolution of the position PDF's and their splitting from an initial unimodal function into bimodal densities at later times. The peaks follow rather closely the two extremal classical solutions, indicated by asterisks on the abscissa. It is notable that there are jump-discontinuities in the PDF's for the spliced potential, which arise from similar jumps in the Jacobians $J_t(x_0)$ for that potential, due to its lower smoothness. See [33] for details. However, qualitatively the PDF evolutions for the first-order spliced potential and the smoother Kummer potential are quite similar. In Fig. 2 we illustrate instead the convergence of the PDF's at fixed time t to a pair of delta functions for $\ell = \sigma \ll x_+(t)$, which is the key signature of QSS. Again the behaviors for the spliced potential and the Kummer potential are quite similar.

These results have interesting implications for the position-space spreading of the initial wavepacket, defined as usual by

$$(\Delta x(t))^2 = \int dx (x - \langle x \rangle)^2 |\psi(x, t)|^2. \quad (25)$$

Using our WKB results, we find that asymptotically at long times $t \gg (\ell^{1-\alpha}/C)^{1/2}$ the spreading is given by

$$(\Delta x(t))^2 \sim \left[\frac{1}{2}(1-\alpha) \left(\frac{2C}{1+\alpha} \right)^{1/2} t \right]^{4/(1-\alpha)}. \quad (26)$$

This is ‘‘Richardson-like’’ not only in that it is a superballistic power-law but, more importantly, in that it is independent of both \hbar and σ , and thus non-vanishing in the mathematical limit of \hbar, σ going to zero. This should be contrasted with the standard result for ballistic position-space spreading of the same initial wavepacket under free-particle dynamics:

$$(\Delta x(t))^2 = \sigma^2 + (ht/2m\sigma)^2.$$

In this case, the spreading vanishes in the limit $\hbar/m \rightarrow 0$ first (WKB limit) and then $\sigma \rightarrow 0$. In fact, this is the usual textbook explanation for classical behavior of very massive particles. It should be remembered that the constant C in (26) is inversely proportional to m , so that the spreading in the cusp potential is also slower for large m , but one can always observe a large spread by waiting a time proportional to $m^{1/2}$ but independent of \hbar .

It is also instructive to compare with the spreading of the Gaussian wave-packet in the power-law potential for $\alpha = 1$, that is, the inverted oscillator potential,

$$V(x) = -\frac{1}{2}Cx^2,$$

which has been very well-studied [44, 45]. The spreading here is:

$$(\Delta x(t))^2 = \sigma^2 \cosh^2(C^{1/2}t) + \left(\frac{\hbar}{2mC^{1/2}\sigma} \right)^2 \sinh^2(C^{1/2}t).$$

This result is easily obtained by analytic continuation of the well-known result for the harmonic oscillator to imaginary frequency. If one takes first the WKB limit $h/m \rightarrow 0$ (or $h/\sqrt{m} \rightarrow 0$, since $C \propto 1/m$) and then $\sigma \rightarrow 0$, the spreading vanishes just as for the free particle. Furthermore, the wavepacket remains unimodal and even Gaussian in the WKB limit since the Jacobian $J_t(x_0) = \cosh(C^{1/2}t)$ is independent of x_0 . In fact, this is exactly true for the full Schrödinger evolution as well [44], and no maxima of $|\psi(x, t)|^2$ at non-zero x ever develop in that case. This example shows that the novel features associated to the cusp potential are due to its “roughness” or non-smoothness and not merely due to strong repulsion from the origin.

We have ignored so far the effect of a large-scale cut-off L to the power-law range of the potential. However, at a time of the order of $(L^{1-\alpha}/C)^{1/2}$ the maxima of $\rho = |\psi|^2$ at $x_{\pm}(t)$ will reach $|x| \simeq L$ and the effects of that cut-off will begin to be felt. At that time the power-law spreading (26) will terminate. The behavior subsequently will depend upon the specific details of the potential at length scales $|x| > L$.

B. Splitting Time

The results of the previous section demonstrate that indeterminacy survives as $\sigma, \ell \rightarrow 0$ or as $t \rightarrow \infty$ in the WKB limit. However, in order to design possible experiments, it is necessary to know exactly how long one must wait to observe such effects. The simplest measure of this is the time of first appearance of new local maxima of ρ at non-zero values of x , i.e. when the wave-function “splits” into multiple peaks. By our previous dimensional analysis, this will occur at a dimensionless time $\tau_c(\mu)$ which will depend upon the parameter μ , which we refer to as the *splitting time*. We can think of the position x of the new maximum as the “order parameter” for transition to QSS at the critical time $\tau_c(\mu)$. All local extrema of the WKB formula $\rho = \rho_0/J$ will occur at $x = x_t(x_0)$ for x_0 satisfying $(\rho_0/J)' = 0$, at points where ρ is differentiable. This gives the condition for a local extremum as

$$J'_t(x_0)/J_t(x_0) = \rho'_0(x_0)/\rho_0(x_0),$$

or as the vanishing of the Wronskian $W(J_t, \rho_0)$.

Because of the symmetry of the classical dynamics around the origin $J'_t(0) = 0$ and because of the symmetry of the initial wavepacket $\rho'_0(0) = 0$ also, so that there is an extremum of $\rho(x, t)$ at $x = 0$ for all times. For the generic case of a symmetric, smooth potential the appearance of the new maxima should appear by a (supercritical) pitchfork bifurcation at $x = 0$, with the origin changing from maximum to minimum and two new maxima appearing to either side. We shall verify this expectation for the Kummer potential. Of course, the pitchfork bifurcation is unstable to any slight asymmetry, in either the potential or initial wavepacket, and will usually be modified then to a saddle-node bifurcation in

which a new maximum-minimum pair appear near (but not exactly at) $x = 0$. The observable consequences are hardly distinguishable from the pitchfork bifurcation for slight asymmetry, so that we analyze only the exactly symmetrical problem here. The first-order spliced potential, although symmetric, exhibits also a saddle-node bifurcation [33]. In that case the Jacobian $J_t(x_0)$ is constant in x_0 very near the origin for all times t (see eq.(23)) and thus the local maximum in ρ_0 at $x = 0$ is preserved in $\rho = \rho_0/J$. This non-generic behaviour occurs because of the lower smoothness of the spliced potential. The peak of ρ at $x = 0$ cannot be easily seen in the numerical solutions presented in the previous section because the height of the peak decreases exponentially in time.

To identify the critical time $\tau_c(\mu)$ one can apply the condition for a degenerate extremum, which is here

$$J''_t(x_0)/J_t(x_0) = \rho''_0(x_0)/\rho_0(x_0).$$

However, in the present case there is a more convenient approach, due to the fact that $-J'_t/J$ increases monotonically in time for $x_0 > 0$. Because of the symmetry of the problem, we can restrict our attention only to positive x_0, x . To demonstrate the monotonicity for $x_0 > 0$, first note using the evolution equations (18) for J, K and similar evolution equations for J', K' [33] that

$$\frac{d}{dt}(K'J - J'K) = -V'''(x)J^3.$$

Since particles in 1D preserve their order, $J > 0$ and thus $d/dt(K'J - J'K) \leq 0$ for potentials of the sort considered here with $V'''(x) > 0$ for $x > 0$. Also, $K'J - J'K = 0$ at $t = 0$ so that

$$\frac{d}{dt}(-J'/J) = -(K'J - J'K)/J^2 \geq 0.$$

Note that generally $-\rho'_0/\rho_0 \geq 0$ at $x > 0$, for initial wavepackets with probability decaying monotonically away from the origin. Also, at time zero $J'/J \equiv 0$, since $J_0(x_0) \equiv 1$. Thus, a simple procedure is to evolve $-J'_t/J_t$ in time and, as it rises upward from zero, identify the first time that its graph touches the graph of $-\rho'_0/\rho_0$.

We can now apply these results to evaluate the splitting time $\tau_c(\mu)$ for the case of a Gaussian wave-packet. Since $-\rho'_0(x_0)/\rho_0(x_0) = x_0/\sigma^2$, the condition for extrema of ρ becomes

$$-J'_t(x_0)/J_t(x_0) = x_0/\sigma^2.$$

It is most convenient to use this condition in a dimensionless form for $u_0 = x_0/\ell$ and $\tau = t/(\ell^{1-\alpha}/C)^{1/2}$, or

$$-J'_\tau(u_0)/J_\tau(u_0) = \mu^2 u_0,$$

with $\mu = \ell/\sigma$. The full analysis of this equation for all μ to find the minimum τ with solutions at positive u_0 requires a numerical study using the method discussed above [33], the results of which are presented in Fig.3. However,

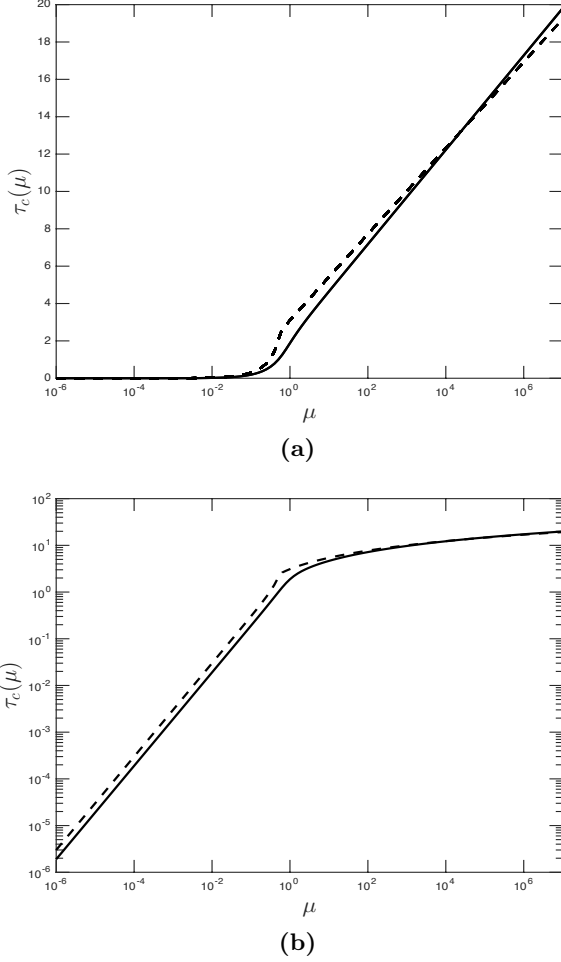


FIG. 3 Splitting time $\tau_c(\mu)$ plotted versus μ , (a) in log-linear and (b) in log-log, for both Kummer potential and 1st-order spliced potential. Notations as in Fig. 1.

analytical results can be obtained asymptotically for $\mu \ll 1$ and $\mu \gg 1$.

We first consider $\mu \ll 1$ for the Kummer potential. One can then just Taylor-expand to get

$$x_t(x_0) = x_0 + \dot{x}_0 t + \frac{1}{2} \ddot{x}_0 t^2 + \dots = x_0 - \frac{1}{2} V'(x_0) t^2 + \dots$$

We note here the convenient formulas [33]

$$V'_\ell(x) = -A_\alpha C \ell^{\alpha-1} x \cdot {}_1F_1\left(\frac{1-\alpha}{2}, \frac{3}{2}; -\frac{x^2}{2\ell^2}\right)$$

$$V''_\ell(x) = -A_\alpha C \ell^{\alpha-1} {}_1F_1\left(\frac{1-\alpha}{2}, \frac{1}{2}; -\frac{x^2}{2\ell^2}\right)$$

$$V'''_\ell(x) = (1-\alpha) A_\alpha C \ell^{\alpha-3} x \cdot {}_1F_1\left(\frac{3-\alpha}{2}, \frac{3}{2}; -\frac{x^2}{2\ell^2}\right)$$

with the dimensionless constant

$$A_\alpha = 2^{(1+\alpha)/2} \Gamma((2+\alpha)/2) / \sqrt{\pi}.$$

Differentiation using the formulas above and non-dimensionalization yields for $\tau \ll 1$

$$-\frac{J'_\tau(u_0)}{J_\tau(u_0)} = \frac{1}{2} V'''(u_0) \tau^2 + \dots$$

Using further the Taylor expansion of the Kummer function ${}_1F_1(a, b; z) = 1 + \frac{a}{b} z + \dots$, gives the result to linear order in τ^2 and cubic order in u_0 :

$$\frac{1}{4} (1-\alpha) \left(1 - \frac{\alpha}{3}\right) A_\alpha \tau^2 u_0^3 = \left(\frac{1}{2} (1-\alpha) A_\alpha \tau^2 - \mu^2\right) u_0.$$

Up to a rescaling of the variables, this is the standard normal form of the pitchfork bifurcation, which is verified by the numerically obtained bifurcation diagram in Fig. 4. There is always the solution $u_0 = 0$, but a symmetrical pair of nonzero solutions appears when the righthand side is positive, i.e. for $\tau > \tau_c(\mu)$ with

$$\tau_c(\mu) \sim \left(\frac{2}{(1-\alpha)A_\alpha}\right)^{1/2} \mu, \quad \mu \ll 1.$$

This asymptotic behavior is verified in the numerical results plotted in Fig.3(b). Note that the linear scaling of $\tau_c(\mu)$ for small μ (but with a different prefactor) will hold for a generic, smooth symmetric potential with $V'''(x) > 0$ for $x > 0$, by the same argument. We also observe in Fig.3(b) the same linear scaling of $\tau_c(\mu)$ for the spliced potential, even though that potential has lower-order smoothness and the bifurcation in that case is an off-origin saddle-node type, as discussed in [33].

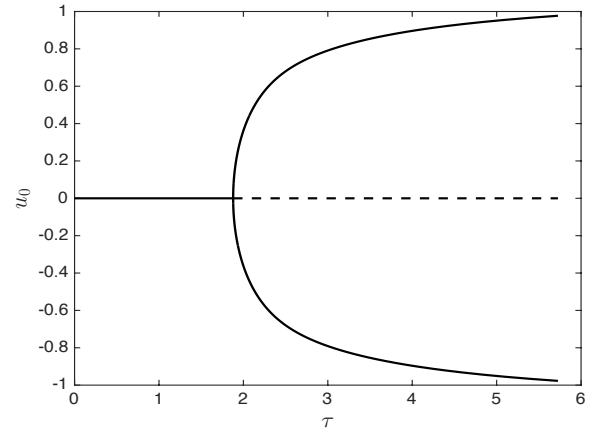


FIG. 4 Bifurcation diagram for the Kummer potential with $\alpha = 1/3$ and for $\mu = 1$, plotting u_0 for all extrema of the WKB position PDF versus dimensionless time τ . Solid lines denote local maxima of the PDF, dashed lines local minima.

We now turn to the limit $\mu \gg 1$. We have found no convenient analytic approach here for the Kummer potential, so that we consider instead the first-order spliced potential, where we can obtain closed expressions for J_t and J'_t/J_t . For $x_0 < \ell$ and $t < t_\ell(x_0)$, one sees easily that

$$J_t(x_0) = \cosh\left(\frac{C^{1/2} t}{\ell^{(1-\alpha)/2}}\right), \quad J'_t(x_0) \equiv 0.$$

For $x_0 < \ell$ and $t > t_\ell(x_0)$, we find that

$$J_t(x_0) = \frac{x_0 x_t}{\bar{x}_0^{1+\alpha} \ell^{1-\alpha}} + \sqrt{x_t^{1+\alpha} - \bar{x}_0^{1+\alpha}} \times \left[-\frac{1}{2}(1-\alpha) \left(\frac{2C}{1+\alpha} \right)^{1/2} (t - t_\ell(x_0)) \frac{x_0}{\bar{x}_0^{1+\alpha} \ell^{1-\alpha}} + \frac{1}{2}(1-\alpha) \left(\frac{2}{1+\alpha} \right)^{1/2} \frac{\ell^{(1+\alpha)/2} \sqrt{\ell^2 - x_0^2}}{x_0 \bar{x}_0^{1+\alpha}} \right].$$

Finally, for $x_0 > \ell$ and all times $t > 0$

$$J_t(x_0) = \frac{1}{x_0} \left[x - (x_+(t))^{(1-\alpha)/2} \sqrt{x_t^{1+\alpha} - x_0^{1+\alpha}} \right].$$

Before proceeding, we note that these latter two expressions exhibit a jump-discontinuity in $J_t(x_0)$ at $x_0 = \ell$, which leads to the discontinuity in the WKB probability density ρ which was observed in the previous section. We also note here that J_t at long times appears to grow $\propto x_+(t)$, but there is in fact a near-cancellation between two terms with such growth. The actual growth is

$$J_t(x_0) \propto [x_+(t)/\ell]^{(1+\alpha)/2} G(x_0/\ell), \quad t \gg (\ell^{1-\alpha}/C)^{1/2}$$

for some explicit function $G(u_0)$ [33]. This result has the interesting implication that the peaks in $\rho(x, t)$ at $x_\pm(t)$ have widths $\propto [x_+(t)]^{(1+\alpha)/2}$ as $t \rightarrow \infty$. However, the scaled density $\hat{\rho}(\hat{x}, \tau)$ has peaks at ± 1 with widths $\propto [x_+(t)]^{-(1-\alpha)/2} \rightarrow 0$ as $\tau \rightarrow \infty$.

It is quite straightforward by differentiating the previous results with respect to x_0 to obtain expressions for $-J'_t(x_0)/J_t(x_0)$. Complete formulas are given in [33], but here we write only the finite limiting result for $\tau \rightarrow \infty$:

$$-J'_\infty(u_0)/J_\infty(u_0) = -\frac{1}{u_0} + \frac{1+3\alpha}{(1-\alpha) + (1+\alpha)u_0^2} + \frac{2}{u_0 \left[1 - u_0^2 + \frac{2}{1-\alpha} \left(\frac{1+\alpha}{2} \right)^{1/2} u_0^2 \sqrt{1 - u_0^2} F(u_0) \right]} \quad (27)$$

with

$$F(u_0) = {}_2F_1 \left(\frac{1}{2}, -\frac{1-\alpha}{2(1+\alpha)}; \frac{1+3\alpha}{2(1+\alpha)}; \frac{(1-\alpha) + (1+\alpha)u_0^2}{2} \right),$$

for $u_0 < 1$, and

$$-J'_\infty(u_0)/J_\infty(u_0) = \frac{1+\alpha}{2} \frac{1}{u_0} \quad (28)$$

for $u_0 > 1$. This function is plotted in Fig.5.

We note that the straight line $\mu^2 u_0$ for $\mu \gg 1$ intersects the curve $-J'_\infty(u_0)/J_\infty(u_0)$ at two non-zero values of u_0 in the range $0 < u_0 < 1$, one near $u_0 = 0$ and another near $u_0 = 1$. Because of the monotonic increase of $-J'_\tau(u_0)/J_\tau(u_0)$ with τ , there are no solutions at any time between these values of u_0 . We can determine the solutions near $u_0 = 0$ and $u_0 = 1$ by considering the behavior of $-J'_\infty(u_0)/J_\infty(u_0)$ near these points. Near $u_0 = 0$,

$$-J'_\infty(u_0)/J_\infty(u_0) \sim \frac{1}{u_0}$$

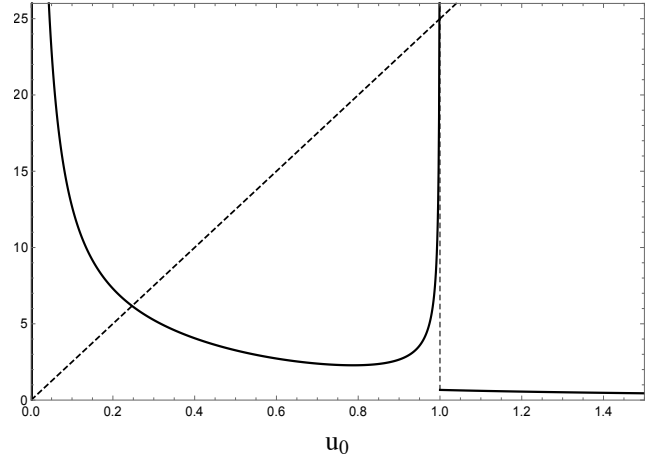


FIG. 5 Plotted versus u_0 are the function $-J'_\infty(u_0)/J_\infty(u_0)$ for the spliced potential with $\alpha = 1/3$, as solid line, and the linear function $\mu^2 u_0$ for $\mu = 5$, as dashed line.

so the solution is at $u_0 \simeq 1/\mu$ and a height μ . On the other hand, near $u_0 = 1$,

$$-J'_\infty(u_0)/J_\infty(u_0) \sim \frac{c}{\sqrt{1 - u_0^2}}$$

for a constant c , so the solution is at $u_0 \simeq 1 - c^2/2\mu^4$ and a height μ^2 . Since the height of the first intersection is much smaller than the height of the second for $\mu \gg 1$, the graph of $-J'_\tau(u_0)/J_\tau(u_0)$ touches the line $\mu^2 u_0$ for a smaller value of τ near the first point $u_0 \simeq 1/\mu$. This cannot happen at any time $\tau < \text{arccosh}(1/u_0)$, because $-J'_\tau(u_0)/J_\tau(u_0) \equiv 0$ before then. This argument yields an exact low bound $\tau_c(\mu) \geq \text{arccosh}(\mu)$. In fact, the graph rises sufficiently rapidly after that time so that

$$\tau_c(\mu) \simeq \text{arccosh}(\mu) \sim \ln \mu, \quad \mu \gg 1;$$

This asymptotic formula agrees with the numerical results on splitting time $\tau_c(\mu)$ for the spliced potential at $\mu \gg 1$ observed in Fig.3(a).

Furthermore, the same logarithmic asymptotics $\tau_c(\mu) \sim \ln \mu$ at large μ appear in the plot for the Kummer potential in Fig.3(a). It is interesting that the same large- μ asymptotics of $\tau_c(\mu)$ hold for the pitchfork bifurcation in the Kummer potential and for the saddle-node bifurcation in the spliced potential. Although we have no proof of this asymptotics for the Kummer potential, there is a simple heuristic argument which leads to this conclusion in both cases. The regime $\mu \gg 1$ corresponds to an initial wavepacket with an extremely narrow spread in position space, $\sigma \ll \ell$, very well localized in the region where the potential appears as an inverted oscillator. However, it is intuitively clear that the splitting of the wavefunction cannot occur until it has spread out of the parabolic region of the potential. In the WKB limit the spreading is due to the classical trajectories, which escape that region exponentially quickly. The time $\tau_c(\mu) \sim \ln \mu$ thus

corresponds to the time it takes for classical particles at distance $\sim \sigma$ from the origin to reach a distance $\sim \ell$.

These findings for $\tau_c(\mu)$ are key results of our paper, providing the time of first onset of quantum spontaneous stochasticity phenomena. The implication is that in the WKB regime this is a short time of order $(\ell^{1-\alpha}/C)^{1/2}$. The longest onset times are for $\mu \gg 1$, but even here the growth of $\tau_c(\mu)$ is only logarithmic, so that QSS phenomena are observable quickly unless the initial wavepacket spread is exponentially small, with $\sigma = e^{-M}\ell$ for $M = \ln \mu \gg 1$.

C. Scattering

We now consider the problem of the scattering of a wavepacket with $\langle x \rangle, \langle p \rangle \neq 0$ when directed toward a UV-cutoff version of the cusp potential (7), which may be easier to study experimentally. To observe QSS in this setting it is clear that the classical dynamics for the initial condition $(\langle x \rangle, \langle p \rangle)$ must reach the phase-point $(x, p) = (0, 0)$, since only here is the flow vector field $\mathbf{U}(x, p)$ for the cusp potential non-Lipschitz. Unlike the problem of turbulent advection where the fluid velocity field is everywhere (nearly) non-Lipschitz, a very careful, fine-tuned choice of $\langle x \rangle, \langle p \rangle$ is here required to observe QSS. The only initial conditions for the unregulated cusp-potential which reach $(0, 0)$ are of the form $(x_+(t), v_-(t))$ and $(x_-(t), v_+(t))$ for some $t > 0$, where $x_{\pm}(t)$ are the extremal solutions given by (9) and $v_{\pm}(t) = dx_{\pm}/dt$. This condition imposes a relation between x and v :

$$v = -\text{sign}(x) \left(\frac{2C}{1+\alpha} \right)^{1/2} |x|^{1+\alpha/2} \quad (29)$$

It is natural to expect that the pair $(\langle x \rangle, \langle v \rangle)$ must be chosen close to a point satisfying (29) in order to observe QSS also for a UV-cutoff version of the cusp-potential.

To verify that this is so, we apply a simple criterion for presence of QSS. In order to have wave-packet splitting in a regulated cusp-potential it is enough to verify that the probabilities for the particle to be found to the left and right of the origin

$$p_-(t) = \int_{-\infty}^0 dx |\psi(x, t)|^2, \quad p_+(t) = \int_0^{+\infty} dx |\psi(x, t)|^2,$$

both remain strictly positive for all times $t \geq t_*$, the splitting time, in the limit $\ell, \sigma \rightarrow 0$. One expects corrections to t_* of order $O((\ell^{1-\alpha}/C)^{1/2})$. These probabilities are easy to evaluate in the WKB limit as

$$p_-(t) = \frac{1}{\sqrt{2\pi}} \int_{-\infty}^{y_*(t)} dy e^{-y^2/2}, \quad p_+(t) = \frac{1}{\sqrt{2\pi}} \int_{y_*(t)}^{\infty} dy e^{-y^2/2},$$

assuming for simplicity a minimum-uncertainty Gaussian initial wavepacket, where

$$y_*(t) = \lim_{\ell, \sigma \rightarrow 0} \left(\frac{x_t^{-1}(0) - \langle x \rangle}{\sigma} \right). \quad (30)$$

and $x_t^{-1}(0) = x_0$ for the initial condition $(x_0, \langle v \rangle)$ which arrives to the origin 0 under the classical dynamics exactly at time t . It follows that, to see wavepacket splitting within WKB, one must have $|y_*(t)| < \infty$ for all $t \geq t_*$.

We can calculate the above quantities analytically for the spliced potential. Note that $x_t^{-1}(0)$ must lie between the origin 0 and $x_{\infty} \equiv x_{\infty}^{-1}(0)$, the point at which a particle with initial velocity $\langle v \rangle$ arrives to the origin only after an infinite time. Energy conservation gives x_{∞} as

$$\frac{C}{1+\alpha} |x_{\infty}|^{1+\alpha} = \frac{1}{2} |\langle v \rangle|^2 + \frac{1}{2} C \ell^{1+\alpha} \left(\frac{1-\alpha}{1+\alpha} \right),$$

since the particle must arrive to 0 with vanishing velocity. If we introduce the position x_* which satisfies the constraint (29) with the velocity $\langle v \rangle$, then this becomes

$$|x_{\infty}|^{1+\alpha} = |x_*|^{1+\alpha} + \frac{1}{2} (1-\alpha) \ell^{1+\alpha}. \quad (31)$$

As expected, $x_{\infty} \rightarrow x_*$ as $\ell \rightarrow 0$. The above derivation has assumed that $|\langle v \rangle| > C \ell^{1+\alpha}$, so that $|x_{\infty}| > \ell$. If instead, $|\langle v \rangle| < C \ell^{1+\alpha}$, then the point x_{∞} lies in the inverted-oscillator region of the spliced potential. In that case it is easy to show again by energy conservation that

$$x_{\infty} = -\langle v \rangle / \gamma,$$

with $\gamma = (C/\ell^{1-\alpha})^{1/2}$.

The classical solution which starts at x_{∞} must spend an infinite amount of time in the inverted-oscillator region $|x| < \ell$ before reaching 0. This can be verified by exactly solving the dynamics in the inverted-oscillator region as

$$x = x_0 \cosh(\gamma t) + \frac{1}{\gamma} v_0 \sinh(\gamma t),$$

so that the particle reaches the origin when $|v_0| > \gamma |x_0|$ and x_0, v_0 have opposite signs, with this process taking a time $t = (1/\gamma) \text{arctanh} |\gamma x_0 / v_0|$. To apply this result to solutions starting at x_0 with $|x_0| > \ell$, we note that such solutions reach distance ℓ from the origin with a velocity $v_{\ell}(x_0)$ given by energy conservation as

$$v_{\ell}^2 = \frac{2C}{1+\alpha} [|x_*|^{1+\alpha} - |x_0|^{1+\alpha} + \ell^{1+\alpha}],$$

or, using (31), as

$$v_{\ell}^2 = (\gamma \ell)^2 + \frac{2C}{1+\alpha} [|x_{\infty}|^{1+\alpha} - |x_0|^{1+\alpha}].$$

Hence the time that classical solutions for such initial positions x_0 spend in the inverted-oscillator region is

$$\tau_{\ell}(x_0) = \frac{1}{\gamma} \text{arctanh} \left(\frac{\gamma \ell}{v_{\ell}(x_0)} \right).$$

For the special case $x_0 = x_{\infty}$, one has $v_{\ell} = \gamma \ell$ and thus the time is infinite, as expected.

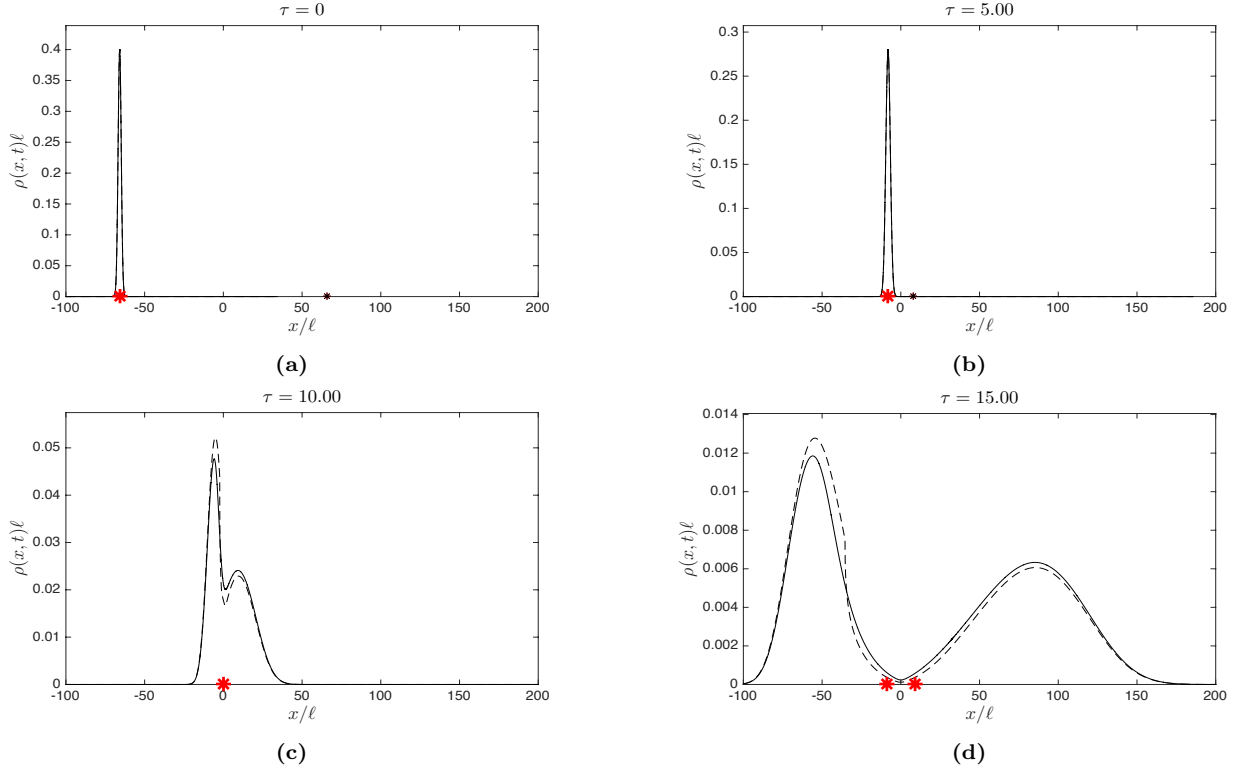


FIG. 6 WKB position-space probability densities for an incoming wave-packet with $\langle v \rangle / (C\ell^{1+\alpha})^{1/2} = 20$, $\langle x \rangle = x_\infty$, and $\sigma = \ell$ at dimensionless times $\tau = 0, 5, 10, 15$. Here $\alpha = 1/3$ and notations are as in Fig. 1. For movie, see [33].

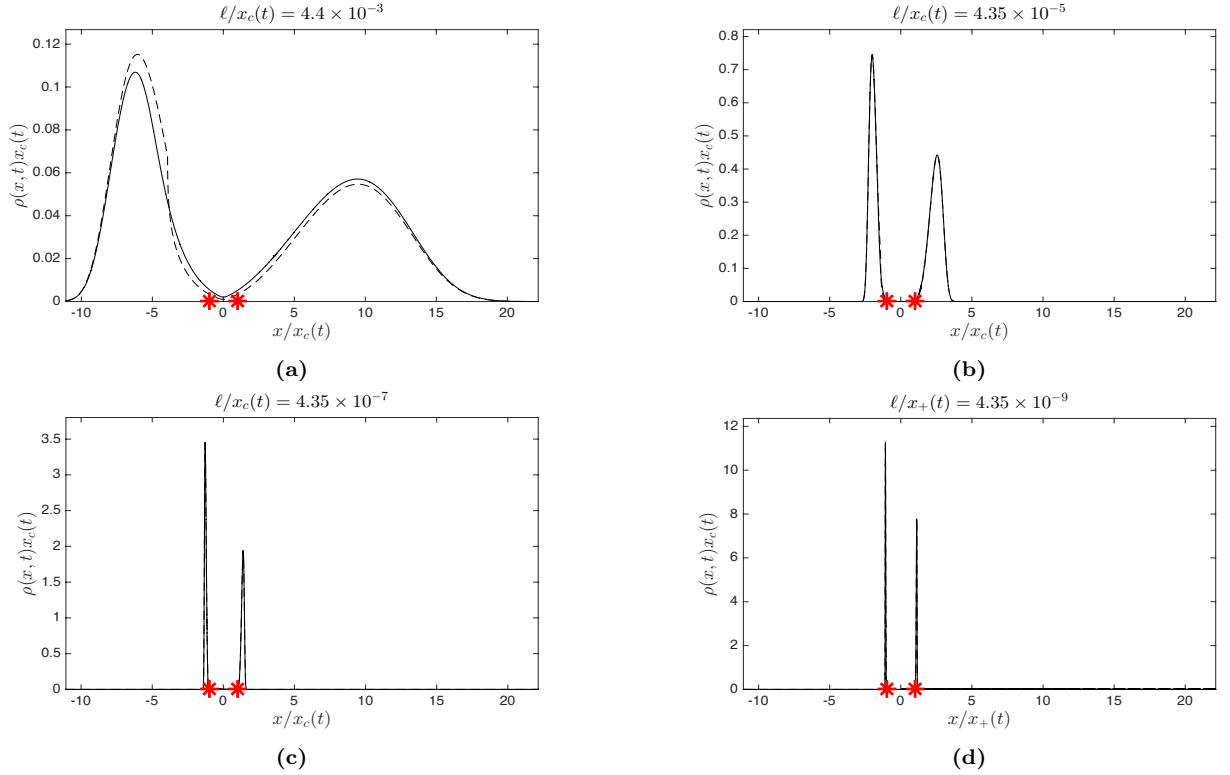


FIG. 7 WKB position-space probability densities for incoming wave-packet with $\langle v \rangle$, $\langle x \rangle$ and time t as in Fig. 6(d), but now with ℓ reduced to give $\ell/x_c(t) = 4.35 \times 10^{-3}, 10^{-5}, 10^{-7}, 10^{-9}$, with notations as in Fig. 1. For movie, see [33].

These considerations fully characterize the value $x_0 \equiv x_t^{-1}(0)$. The important constraint comes from the solu-

tion (11) for the dynamics in the cusp-region $|x| > \ell$ of the potential. Using this equation for final position $|x| = \ell$ and time $t - \tau_\ell(x_0)$ to reach that point yields

$$\begin{aligned} & \ell^{(1-\alpha)/2} {}_2F_1\left(\frac{1}{2}, -\frac{(1-\alpha)}{2(1+\alpha)}; \frac{1+3\alpha}{2(1+\alpha)}; + \left|\frac{\bar{x}_0}{\ell}\right|^{1+\alpha}\right) \\ & - |x_0|^{(1-\alpha)/2} {}_2F_1\left(\frac{1}{2}, -\frac{(1-\alpha)}{2(1+\alpha)}; \frac{1+3\alpha}{2(1+\alpha)}; + \left|\frac{\bar{x}_0}{x_0}\right|^{1+\alpha}\right) \\ & = -\frac{1}{2}(1-\alpha)\left(\frac{2C}{1+\alpha}\right)^{1/2} (t - \tau_\ell(x_0)). \end{aligned} \quad (32)$$

Here we have assumed a negative-energy solution appropriate to a point near x_∞ and taken a minus sign on the righthand side for the case $\text{sign}(x_0 \cdot \langle v \rangle) = -1$. To evaluate $x_0 = x_t^{-1}(0)$ asymptotically for small ℓ it is convenient to parameterize this solution by the dimensionless quantity $\xi > 0$ introduced through the formula

$$|x_0|^{1+\alpha} = |x_\infty|^{1+\alpha} - \xi \ell^{1+\alpha}. \quad (33)$$

In terms of this parameter $v_\ell^2 = C \frac{1+\alpha+2\xi}{1+\alpha}$ and

$$\tau_\ell(\xi) = \frac{1}{\gamma} \text{arctanh} \sqrt{\frac{1+\alpha}{1+\alpha+2\xi}}. \quad (34)$$

Also the quantity \bar{x}_0 appearing in (32) must be chosen according to the condition

$$H_0 = -\frac{C}{1+\alpha} |\bar{x}_0|^{1+\alpha} = \frac{1}{2} v_\ell^2 - \frac{C}{1+\alpha} \ell^{1+\alpha}$$

which gives

$$|\bar{x}_0|^{1+\alpha} = \left[\frac{1}{2}(1-\alpha) - \xi \right] \ell^{1+\alpha}. \quad (35)$$

With these choices $x_0 = x_t^{-1}(0)$ is the solution of the fixed-point condition (32).

We can now evaluate the solution asymptotically as $\ell \rightarrow 0$. Because $\gamma \rightarrow \infty$ in that limit, the only way to satisfy (34) for a fixed finite value $\tau_\ell(\xi) = \tau > 0$ is to choose the parameter ξ exponentially small:

$$\xi \doteq 2(1+\alpha)e^{-2\gamma\tau}.$$

This implies that x_0 in (33) must be exponentially close to x_∞ and, in particular, $x_0 \rightarrow x_*$, verifying our original expectation. Furthermore from (35)

$$\left|\frac{\bar{x}_0}{\ell}\right|^{1+\alpha} \rightarrow \frac{1}{2}(1-\alpha),$$

and from (35),(33)

$$\left|\frac{\bar{x}_0}{x_0}\right|^{1+\alpha} = O\left(\left|\frac{\ell}{x_*}\right|^{1+\alpha}\right) \rightarrow 0.$$

These results in the fixed-point condition (32) give

$$O(\ell^{(1-\alpha)/2}) + |x_*|^{(1-\alpha)/2} = \frac{1}{2}(1-\alpha)\left(\frac{2C}{1+\alpha}\right)^{1/2} (t - \tau_\ell),$$

which can only hold if $t - \tau_\ell = t_* + O((\ell^{1-\alpha}/C)^{1/2})$, where t_* is the time given by the relation

$$|x_*| = \left[\frac{1}{2}(1-\alpha)\left(\frac{2C}{1+\alpha}\right)^{1/2} t_* \right]^{2/(1-\alpha)},$$

or the time t_* required for the extremal solutions (9) of the cusp-potential to transit from x_* to 0. We conclude that $x_0 = x_t^{-1}(0)$ for the spliced-potential is given by

$$|x_0|^{1+\alpha} \doteq |x_\infty|^{1+\alpha} - 2(1+\alpha)e^{-2\gamma(t-t_*)}\ell^{1+\alpha} \quad (36)$$

in the limit $\ell \rightarrow 0$, for x_∞ in (31) and $\gamma = (C/\ell^{1-\alpha})^{1/2}$, for all $t \geq t_*$. The simple picture that emerges here is that solutions starting at $x_0 = x_t^{-1}(0)$ given by (36) reach a distance ℓ from the origin in a time $\simeq t_*$, nearly independent of ℓ , and then take an additional time $\simeq \tau = t - t_*$ to reach the origin, for a total time t . This is made possible by the fact that extremal solutions (9) of the cusp-potential transit between x_* and 0 in a finite time t_* , as a consequence of the non-smoothness of that potential.

With these results in hand, we can now discuss the wavepacket scattering in the WKB limit. With the mean velocity $\langle v \rangle$ fixed, there are various possible choices of $\langle x \rangle$ to observe splitting of the wavepacket and QSS. For example, one may choose $\langle x \rangle = x_\infty$. Since (36) implies

$$x_t^{-1}(0) \doteq x_\infty \left[1 - 2e^{-2\gamma(t-t_*)} \left| \frac{\ell}{x_*} \right|^{1+\alpha} \right],$$

almost any reasonable choice of σ , e.g. $\sigma \propto \ell^p$ for any power p , will give

$$y_*(t) = 0, \quad t \geq t_*.$$

This corresponds to a symmetrical splitting, with both $p_-(t) = p_+(t) = \frac{1}{2}$ for $t \geq t_*$. Another natural choice is $\langle x \rangle = x_*$. Using (36),(31), it follows that

$$x_t^{-1}(0) \doteq x_* \left[1 + \frac{1-\alpha}{2(1+\alpha)} \left| \frac{\ell}{x_*} \right|^{1+\alpha} \right],$$

so that taking $\sigma = \beta \ell^{1+\alpha}/|x_*|^\alpha$ gives

$$y_*(t) = \frac{1}{2\beta} \frac{1-\alpha}{1+\alpha} \text{sign}(x_*), \quad t \geq t_*.$$

Hence $p_+(t) = \frac{1}{2} \text{erfc}(\frac{\pm 1}{2^{3/2}\beta} \frac{1-\alpha}{1+\alpha})$ for $t \geq t_*$ in terms of the complementary error function, corresponding to an asymmetrical splitting. Still another possible choice is $\langle x \rangle = x_* - \kappa\sigma$ for any σ vanishing more slowly than $\ell^{1+\alpha}$, so that $\ell^{1+\alpha}/\sigma \rightarrow 0$ as $\ell \rightarrow 0$. In this case

$$y_*(t) = \kappa, \quad t \geq t_*.$$

and $p_+(t) = \frac{1}{2} \text{erfc}(\kappa)$ for $t \geq t_*$. This would hold with the choice $\sigma = \ell/\mu$ of the previous section, for μ fixed. Although there seem to be a plethora of possibilities, they

are actually quite restricted since one must always make a careful fine-tuning so that $\langle x \rangle \rightarrow x_*$ as $\ell \rightarrow 0$ in order to observe QSS in the scattering process for fixed $\langle v \rangle$.

We now present numerical WKB results for scattering of a wave-packet off both the Kummer potential and the spliced potential. Here we shall consider only the choice $\langle x \rangle = x_\infty$ for fixed $\langle v \rangle$ and $\sigma = \ell$, based upon the analytical results for the sliced potential. Using the same choices for the Kummer potential is a good test on the robustness of the derived selection criteria for small changes in the regularization of the potential. (Note that one could also make an alternative choice of x_∞ for the Kummer potential by using its own energy conservation law to choose the position of the particle with velocity $\langle v \rangle$ which arrives to the origin with zero velocity.) We consider first the choice $\alpha = 1/3$ and $\langle v \rangle / (C\ell^{1+\alpha})^{1/2} = 20$ so that $x_\infty/\ell \doteq -66.05$ and $\tau_* = t_*/(\ell^{1-\alpha}/C)^{1/2} \doteq 9.902$. In Fig. 6 we show the time-evolution of the WKB position PDF by plotting it at four successive choices of the dimensionless time τ . The classical solution with which we now compare is $x_c(t) = x_\pm(|t - t_*|)$, $\pm = \text{sign}(t - t_*)$, which is incoming as x_- and outgoing as x_+ . We see that the PDF's for both potentials evolve very similarly and split at a time near t_* . It is notable that in the final frame for $\tau = 15$, the probabilities p_-, p_+ are nearly equal to the symmetrical value $1/2$ but the shapes of the peaks on the left and right are different. Next we study the effect of decreasing values of $\sigma = \ell$. In Fig. 7 we fix $\langle v \rangle$, $\langle x \rangle = x_\infty$, final time t , and position $x_c(t)$ from the last panel in Fig. 6 and successively reduce $\ell/x_c(t)$. There is clear evidence of QSS, with the PDF converging to a pair of delta-functions. Even though $p_+, p_- \rightarrow 1/2$, the shape asymmetry of the PDF peaks remains. The most important observation is that the results for the Kummer and spliced potentials are quite similar, giving hope that our selection criterion, although derived rigorously only for the spliced potential, will apply more generally. Other choices of the fine-tuning of the initial wave-packet are implemented by the codes in [33].

V. NUMERICAL SCHRÖDINGER EVOLUTION

Thus far, we have considered a WKB regime in which, formally, the limit $h/m \rightarrow 0$ is taken first with position spread $\Delta x_0 = \sigma$ of the wavepacket fixed and then subsequently letting $\sigma \rightarrow 0$. However, this is not the only limit in which deterministic classical dynamics is generally expected to emerge. One can also let h/m and Δx_0 go to zero together, e.g. with position spread $\Delta x_0 \propto (h/m)^\beta$ and velocity spread $\Delta v_0 \propto (h/m)^{1-\beta}$ for any $0 < \beta < 1$, consistent with the Heisenberg uncertainty relations. For general smooth potentials and for an initial minimum-uncertainty wavepacket with $\Delta x_0, \Delta v_0$ chosen as above, it can be shown that the position and velocity spreads $\Delta x_t, \Delta v_t$ at later times t vanish for the limit $h/m \rightarrow 0$ and the mean values $\langle x \rangle_t, \langle v \rangle_t$ evolve according to the classical dynamics [46]. Note that WKB corresponds to

the special case $\beta = 0$. However, if the potential is rough down to a length-scale ℓ and if $\ell \rightarrow 0$ as $h/m \rightarrow 0$, then particle motion could remain stochastic in any of these alternate classical limits as well.

To give a careful formulation of such alternative semi-classical limits, we define a “dimensionless- \hbar ” parameter

$$\varepsilon = \frac{\hbar}{mC^{1/2}\delta^{(3+\alpha)/2}}, \quad (37)$$

where δ is some suitable macro-length scale, which could be the outer length L of the potential, the length D of the space domain, or some specified fraction of either of these lengths. The quantity defined in (37) thus corresponds to the “inverse Péclet number” κ/UL in terms of the turbulent advection - quantum mechanics analogy discussed in Section III. The alternative semi-classical limits are then defined by taking $\varepsilon \ll 1$ with

$$\sigma = \ell/\mu, \quad \ell = \delta \cdot \varepsilon^\beta, \quad 0 < \beta < 1.$$

This choice of ℓ gives the potential additional mass-dependence beyond that in the prefactor $C \propto 1/m$. If the Schrödinger equation (19) is non-dimensionalized by introducing $\tilde{x} = x/\delta, \tilde{t} = t/(\delta^{1-\alpha}/C)^{1/2}$, then it becomes

$$i\varepsilon\partial_{\tilde{t}}\psi = -\frac{\varepsilon^2}{2}\Delta_{\tilde{x}}\psi + \tilde{V}(\tilde{x})\psi \quad (38)$$

with now $\tilde{m} = \tilde{C} = \tilde{\delta} = 1$ and $\tilde{\ell} = \varepsilon^\beta$ for $\varepsilon \ll 1$.

We numerically study the semi-classical limit in the setting described above with $\beta = 1/2$ and $\delta = D/128\pi$. We modified a publicly available code [47] to solve the Schrödinger equation in one dimension for the Kummer potential (12), in the dimensionless formulation (38). The code `pySchrodinger` employs the so-called Strang operator-splitting spectral method, which is especially suitable for the semi-classical limit problem [48]. This approximation introduces second-order time-discretization errors by time-splitting, but has exponential accuracy in spectral computation of spatial derivatives for sufficiently smooth wave-functions. It has the great advantage of giving evolution which is unitary, time-reversible, and gauge-invariant under spatially constant shifts in the potential, to machine precision. In the numerical experiments presented here we study an initial minimum-uncertainty wave-packet with $\langle \tilde{x} \rangle = \langle \tilde{v} \rangle = 0$ and $\mu = 1$, making a sequence of runs with $\varepsilon = 2^{-n}$ for all integers $-7 \leq n \leq 10$. We resolve both the spatial and temporal grid to $O(\varepsilon)$ and performed refinement studies to verify that our numerical simulations are converged.

In Fig. 8 we show for $\varepsilon = 2^{-7}$ a sequence of snapshots at successive times of the position-space PDF, along with the positions of the extremal classical solutions. Just as in the WKB limit, the PDF splits into a bimodal distribution at an early time and with the two peaks closely tracking the extremal classical solutions.

We can also study splitting in momentum-space by taking the Fourier transform of the wave-function, de-

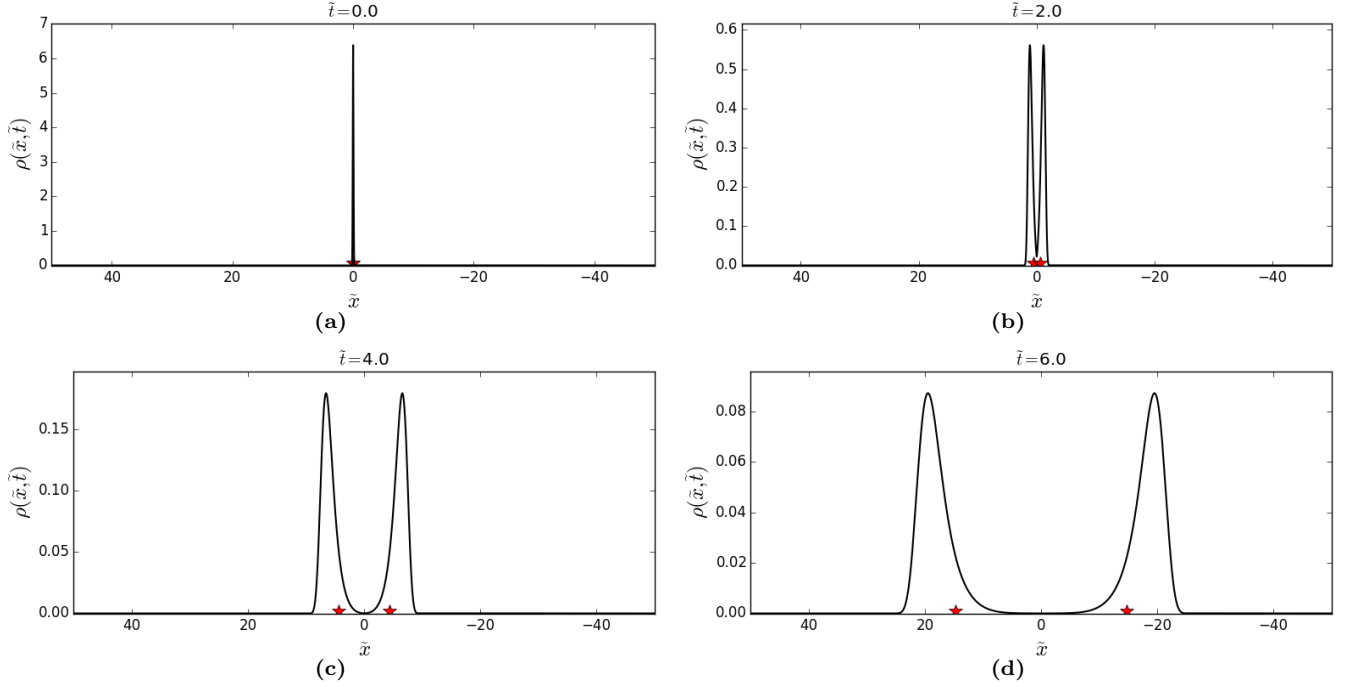


FIG. 8 Position-space PDF for numerical Schrödinger solution with $\varepsilon = 2^{-7}$, at successive times $\tilde{t} = 0, 2, 4, 6$. Asterisks on the abscissa denote positions of the extremal classical solutions. For movie, see [33].

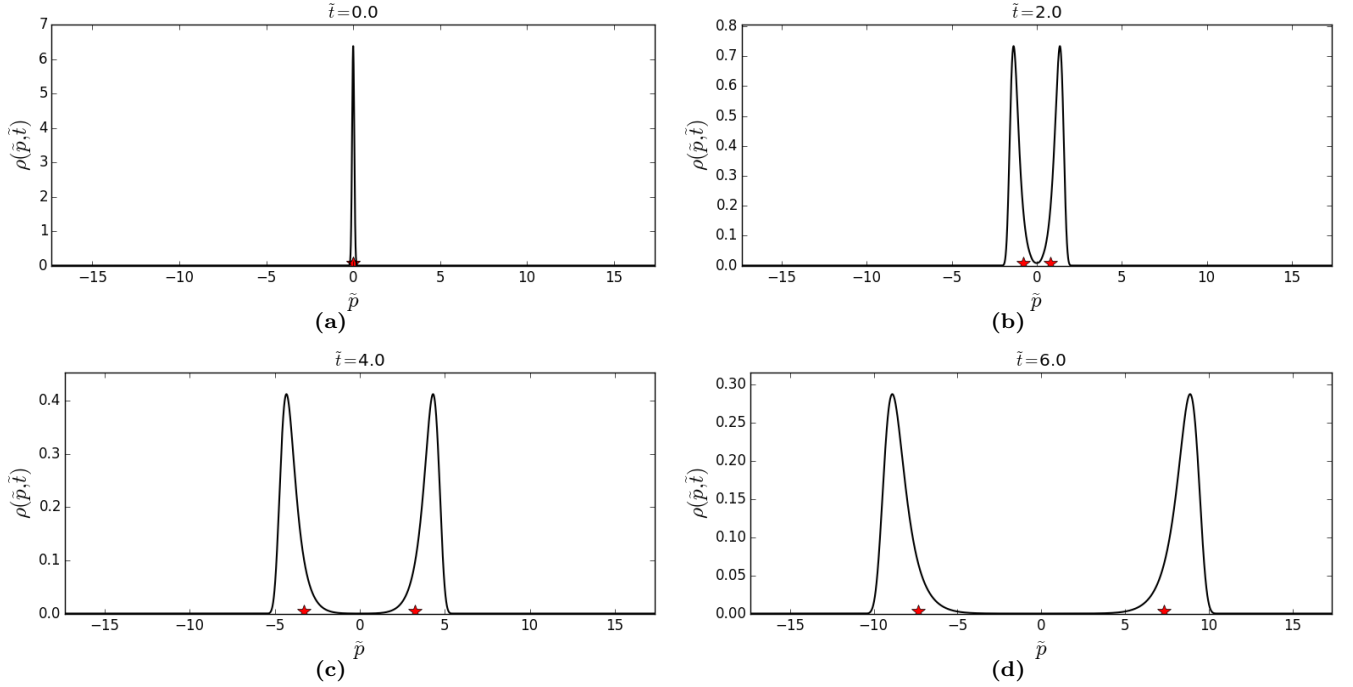


FIG. 9 Momentum-space PDF for numerical Schrödinger solution with $\varepsilon = 2^{-7}$, at successive times $\tilde{t} = 0, 2, 4, 6$. Asterisks on the abscissa denote momenta of the extremal classical solutions. For movie, see [33].

finied in dimensionless form by

$$\hat{\psi}(\tilde{p}, \tilde{t}) = \frac{1}{\sqrt{2\pi\varepsilon^2}} \int d\tilde{x} \psi(\tilde{x}, \tilde{t}) e^{-i\tilde{x}\tilde{p}/\varepsilon}$$

and implemented numerically by a fast Fourier transform (FFT). The momentum-space PDF $\rho(\tilde{p}, \tilde{t}) = |\hat{\psi}(\tilde{p}, \tilde{t})|^2$ is plotted in Fig. 9 for the same cases as in the preceding Fig. 8. For comparison, we also plot the momenta

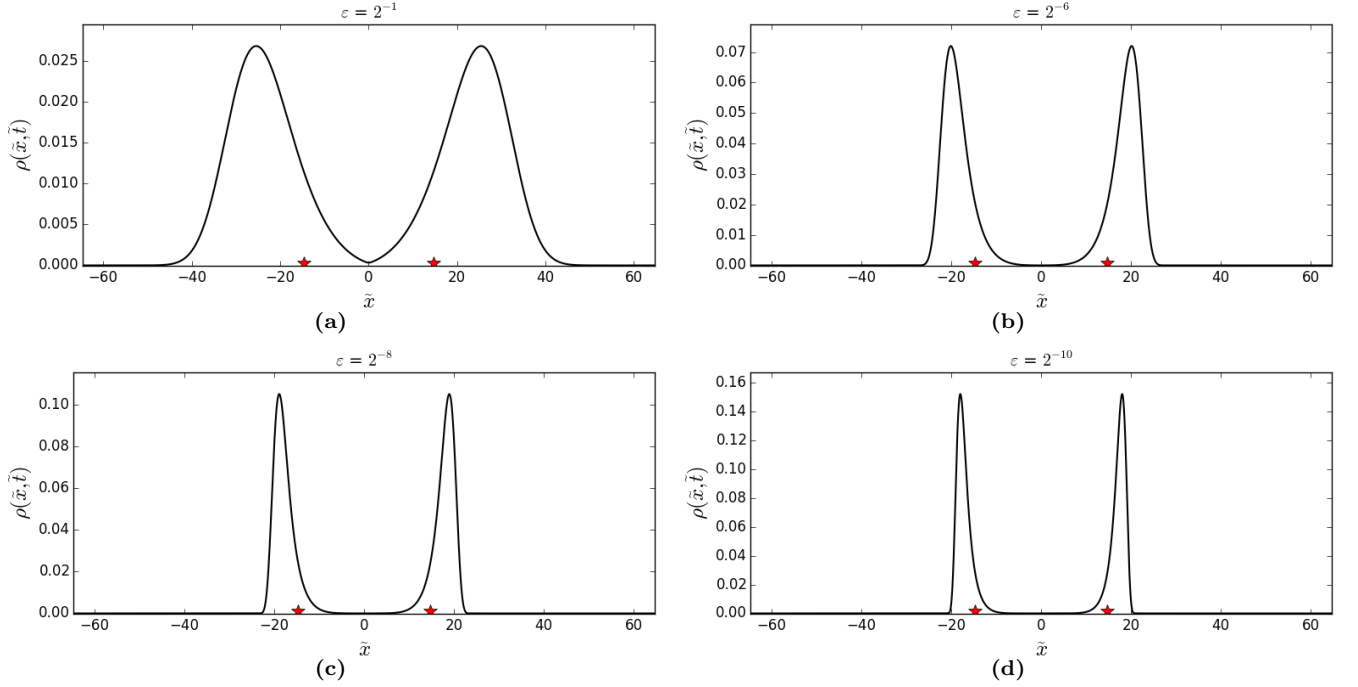


FIG. 10 Position-space PDF for Schrödinger solution at $\tilde{t} = 6$, for $\varepsilon = 2^{-1}, 2^{-6}, 2^{-8}, 2^{-10}$, with notations as in Fig. 8. For movie, see [33].

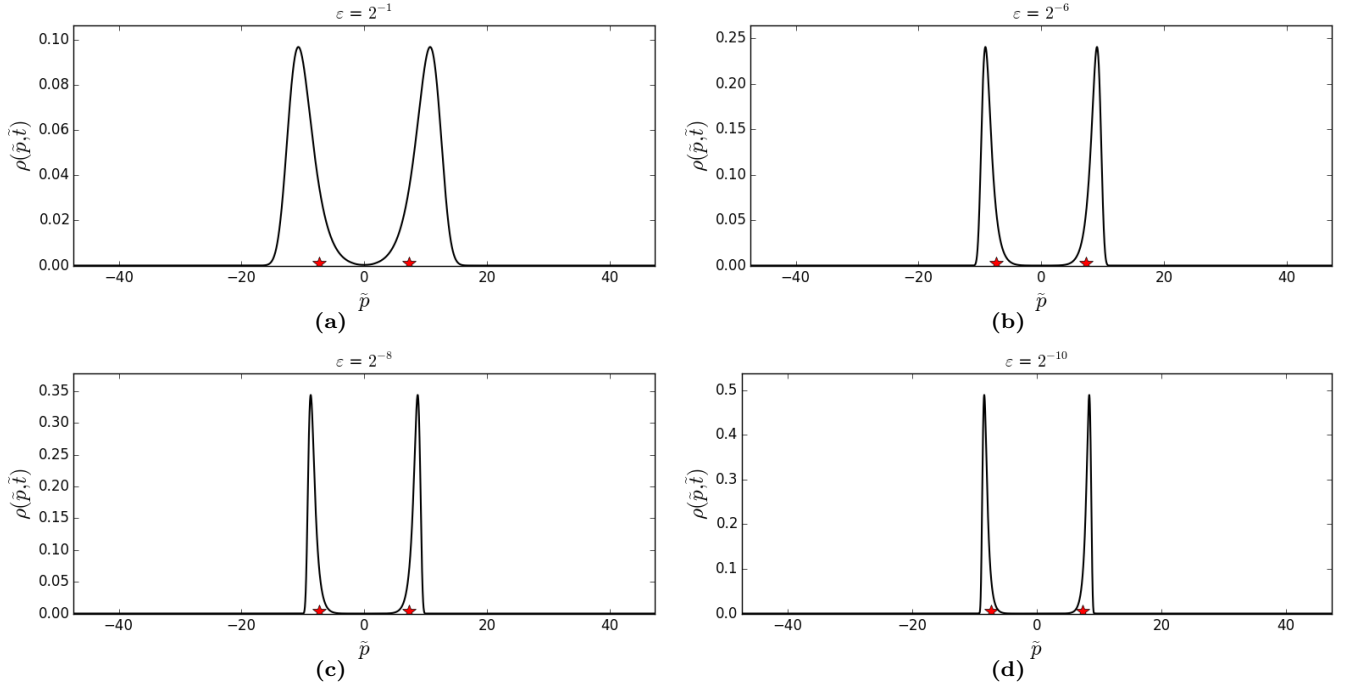


FIG. 11 Momentum-space PDF for Schrödinger solution at $\tilde{t} = 6$, for $\varepsilon = 2^{-1}, 2^{-6}, 2^{-8}, 2^{-10}$, with notations as in Fig. 9. For movie, see [33].

$p_{\pm}(t) = mv_{\pm}(t)$ of the extremal classical solutions in non-dimensionalized form. We see that there is splitting of the wave-packet also in momentum-space and the two peaks of the momentum-space PDF closely track the

momenta of the extremal classical solutions. Although we did not show it earlier, one can obtain similar results for the WKB limit. Numerically, the WKB wavefunction can be interpolated to a regular space grid with spacing

$O(\varepsilon)$ and then transformed by FFT. One observes the same splitting in momentum-space there.

We also study the behavior of the position-space and momentum-space probability distributions at a fixed time t and $\ell = \sigma \propto \varepsilon^{1/2}$ for a decreasing sequence of ε values. The results are presented in Figs. 10-11. In the semiclassical limit $\varepsilon \ll 1$, the probability densities increasingly concentrate around the positions and momenta of the two extremal classical solutions, providing good evidence of QSS in both position-space and momentum-space. We can quantify this further by calculating the position- and momentum-space uncertainties as a function of ε at the same fixed time t . These results are shown in Fig. 12. The horizontal lines are the corresponding theoretical predictions from (26) for the classical dispersion. We see a definite tendency of the numerical uncertainties to converge to their theoretical limit and, most importantly, become asymptotically independent of ε , corroborating the visual evidence in Figs. 10-11.

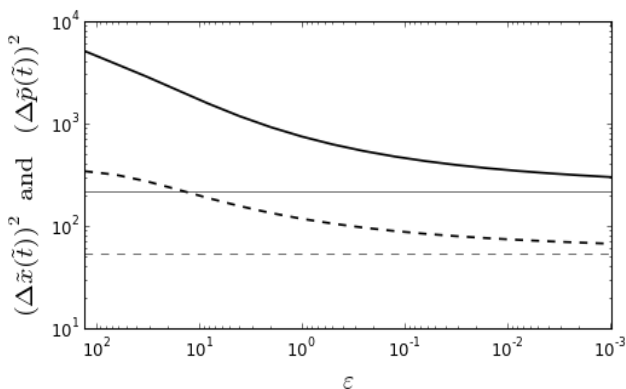


FIG. 12 Uncertainties of position and momentum at the fixed time t in Figs. 10-11, as functions of ε . The heavy solid curve is the numerical position-space dispersion as defined by Eq. (25) and the light solid line is the position dispersion of the two classical extremal solutions (26). The thick dashed curve is the numerical momentum-space dispersion and the thin dashed line is the momentum dispersion of the two classical extremal solutions.

The previous results show that quantum systems may remain stochastic (“God still throws dice”) in the classical limit, where determinism is expected. However, it might appear, even more shockingly, that the particle models discussed here become increasingly accurately described as two-state quantum systems in the limit $\hbar/m \rightarrow 0$, with just two possible values for the position (or momentum). If so, then it could be possible by experimental design of such systems to construct a massive “Schrödinger cat” with arbitrarily large m ! The key question here is whether it is possible to achieve a coherent superposition of the two different states of the particle, leading to quantum interference effects. If there is no such coherence, then any linear superposition of the two possible states really corresponds just to a statistical

mixture within classical probability theory.

There are compelling reasons for lack of coherent superpositions, arising from the quantum uncertainty relations. Note that coherence would require separately for each branch of a “split” wavefunction that the position-space spread be comparable to the de Broglie wavelength, $\Delta x \sim \lambda$. Otherwise, the phase of each branch wavefunction would oscillate rapidly within its envelope of width Δx and the two branches, even if spatially recombined, would have overlap nearly zero. In that case, no interference between them could ever be observed. However, choosing $\Delta x \sim \lambda \propto \hbar/m$ in each branch leads by the uncertainty relations to $\Delta v = O(1)$ for each branch individually and thus very rapid spatial spreading. In the limits where classical dynamics is expected, $\Delta x \gg \lambda$, and thus no coherence of the branches. Hence, the QSS phenomenon allows indeterminism in the classical limit but not quantum superpositions or entanglement.

These arguments can be verified using our numerical Schrödinger solutions. Although the two individual peaks of the position-space PDF in Fig. 10 become increasingly narrow $\propto \varepsilon^{1/2}$ as $\varepsilon \rightarrow 0$, they in fact contain increasingly rapid oscillations on the scale of the de Broglie wavelength $\sim O(\varepsilon)$. We show this in Fig. ?? by zooming in on one of the two peaks (the rightmost) and plotting the function $|\text{Re}(\psi)|^2 = \rho \cos^2(\varphi)$, whose envelope is the position-space PDF but which oscillates with the complex phase φ of the wave-function. Clearly, the wave-functions become extremely oscillatory within the envelope of a single peak as ε is decreased. This rapid phase oscillation renders the two branches of the wave-function decoherent, as it becomes impossible in practice to recombine them spatially in phase. This is also a feature of the WKB wave-function studied previously, as can be seen by calculating its phase $S_t(x)$, the classical action (16), and observing that it grows with increasing mass m of the particle.

VI. POSSIBLE EXPERIMENTS

Such indeterministic, stochastic behavior persisting in the standard classical limits should be observable in laboratory experiments. We have examined in this paper only the simplest 1D model which exhibits the QSS phenomenon and it may not be the easiest to situation to study experimentally. However, the results will readily extend to higher-dimensional cases that may be easier to create in the laboratory. The main requirement is that the repulsive potential of the quantum particle should be (nearly) non-smooth at the maximum energy location. For example, the radially symmetric version of the cusp function (7) as potential energy per unit mass, i.e.

$$V(\mathbf{x}) = -\frac{C}{1+\alpha} r^{1+\alpha}, \quad r = |\mathbf{x}|,$$

will lead to the same QSS phenomena. By standard arguments, the 3D Schrödinger equation for an angular mo-

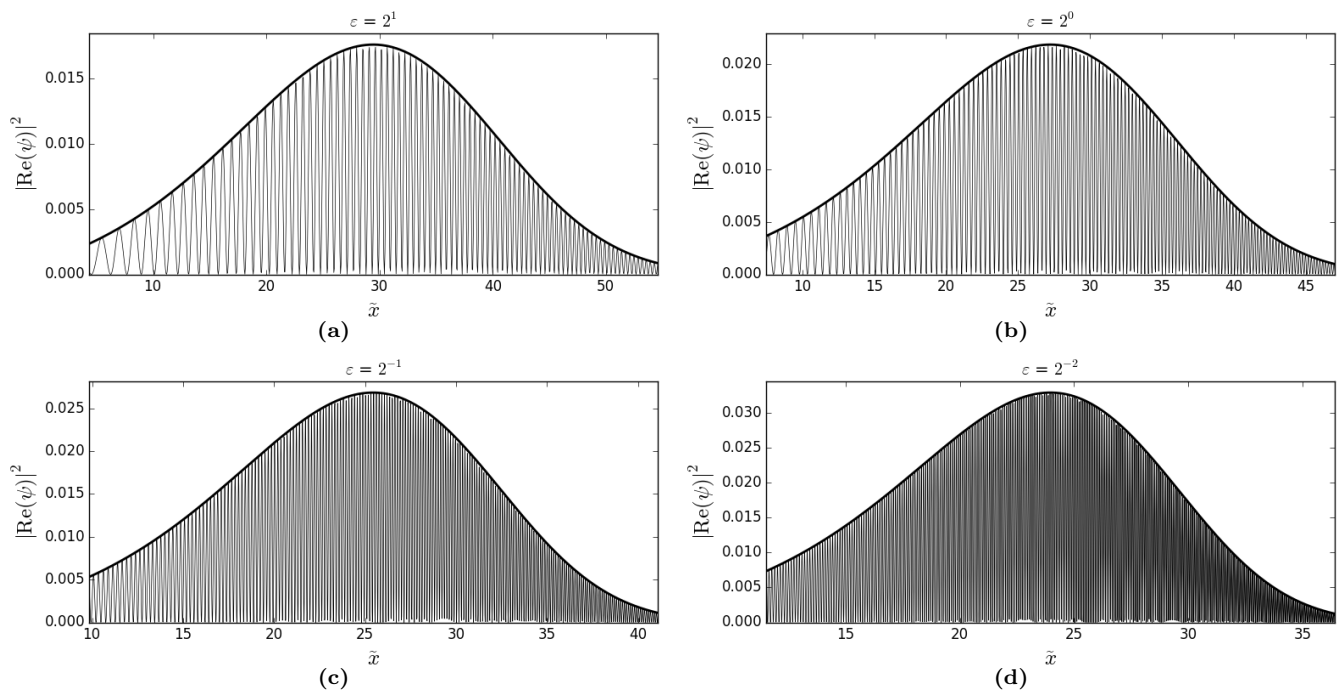


FIG. 13 Plot of $|\text{Re}(\psi)|^2$ near the right peak of the position-space PDF, for $\varepsilon = 2^1, 2^0, 2^{-1}, 2^{-2}$, as light black line. The solid black curve is the plot of the position-space PDF ρ , the envelope of the first graph. Each plot window height is a fixed multiple of the maximum value of the peak and each window width is a fixed multiple of the peak half-width.

momentum ℓ initial wave-packet will reduce to a 1D equation with an effective potential $V_{\text{eff}}(r) = V(r) + \frac{\hbar^2 \ell(\ell+1)}{2mr^2}$. In particular, for an initial $\ell = 0$ wavepacket concentrated at the origin, the analysis in this paper carries over and predicts a spherical wave of probability amplitude radiating from the origin in the standard classical limits where one naively expects the particle to remain sitting at the unstable maximum at the origin. In this case, the randomness involves a continuous infinity of random outcomes, corresponding to the possible directions of the outgoing particle, not just two as in the 1D model.

To verify the phenomenon as QSS, there are key signatures for the experimentalist to check. First, there should be super-ballistic power-law spreading of the wavepacket as in (26). Second, this spreading should be independent of the initial width of the wavepacket σ and inner cutoff ℓ of the potential as those are decreased (but still much larger than the de Broglie wavelength). Third, the spreading should be independent of \hbar/m , which may be testable in some experiments by considering particles with differing masses. (Actually in a fixed potential, there will be a particular mass-dependence, through C or classical inertial effects, rather than strict independence.) It may be easier for experimentalists to observe the corresponding signatures for momentum-space spreading, as discussed in section V. Any experiment attempting to observe QSS will need low temperatures and low levels of other sources of noise, to ensure that quantum fluctuations are driving the phenomenon. We consider here

briefly three possible experimental realizations: ultra-cold AMO, ultra-cold neutrons, and optical analogues.

Ultra-cold atomic-molecular-optical (AMO) systems exhibit quantum evolution of neutral particles in an electric dipole potential created by the AC Stark effect [49, 50]. This potential has the form

$$V(\mathbf{x}) = \frac{3\pi c^2 \Gamma}{2\omega_0^3 \Delta} I(\mathbf{x})$$

where ω_0 is the optical transition frequency, Γ is the damping rate corresponding to the spontaneous decay of the excited level, $I(\mathbf{x})$ is the spatial intensity of the laser light with frequency ω , and $\Delta = \omega - \omega_0$ is the detuning parameter. Achievable potentials have only a small energy scale (mK), but there is great flexibility in designing their spatial form (e.g. see [51, 52]). Attractive electric dipole potentials are widely used to create particle traps for atomic bose-condensates and for quantum computing. A stationary repulsive potential for study of QSS could be accomplished with a blue-detuned ($\Delta > 0$) focused beam or red-detuned ($\Delta < 0$) hollow beam. The QSS phenomenon requires a large scale ratio, $L/\ell \gg 1$, say, $L/\ell \gtrsim 100$, which could be achieved perhaps with large-aperture lasers or a large number of individual beams. To get the cusp-potential would require a fine control of the spatial intensity distribution $I(\mathbf{x})$, so that a power-law such as $I(\mathbf{x}) \propto |\mathbf{x}|^{1+\alpha}$ could be obtained to a suitable approximation. The effects described here should not require an exact power-law but could have discrete

steps of intensity or some rapid variation that averages out on the dynamical times scales of the particle. To achieve such a spatial distribution, one might use methods employed for quantum computing applications, such as artificial holograms with acousto-optic deflectors [51], spatial light modulators [52], or other devices. In contrast to quantum computing applications, one does not require rapid manipulation and control of potentials, but instead accurate specification of the intensity spatial distribution over a broad enough region. This seems a very promising approach to explore QSS in the laboratory.

Another possible system with which to realize QSS is ultra-cold neutrons [53–55]. These have energies 1-1000 neV, temperatures \sim mK, de Broglie wavelengths $\lambda = 10$ -1000 nm, velocities $v \sim 5$ m/s. Neutrons interact through all four fundamental forces—strong, weak, electromagnetic and gravitational—which provide various methods to generate potentials acting upon them.

One possibility is the magnetic dipole potential due to an external magnetic field, $V(\mathbf{x}) = -\boldsymbol{\mu} \cdot \mathbf{B}(\mathbf{x})$, which acts on the neutron dipole moment with $\mu = 60$ neV/T. (Magnetic dipole forces are also an option for AMO systems). Magnetic field strengths B as large as 30 T are currently achievable with superconducting magnets and generally somewhat smaller strengths ~ 1 T for permanent magnets. Unless magnetic fields change very rapidly, the alignment of neutron polarization generally follows adiabatically the local magnetic direction, with no spin flips. Thus the dipole interaction is repulsive for spins aligned or magnetic moments anti-aligned with the field (low-field seeking, LFS, state), and attractive for spins anti-aligned/moment aligned (high-field seeking, HFS, state). Magnetic bottles for spin-polarized neutrons, as originally proposed in [56], have been achieved for both LFS and HFS spin states and for electromagnetic and permanent magnets. See e.g. [57] for many references. One could, in principle, use similar methods to generate a (UV-regulated) cusp potential. An advantage of this approach is that magnetic interactions are ideal conservative and relatively “clean” compared to methods involving material mirrors/walls. However, it is difficult for us to conceive of a practical arrangement of permanent magnets and electric currents that would produce a cusp-like potential, with sufficient accuracy.

It is also possible to exploit gravity, since ultra-cold neutrons have kinetic energies comparable to their gravitational potential energies (102 neV per meter height). This can be done in conjunction with material mirrors (essentially, the strong interaction with the atomic nuclei, modelled by nuclear optical potentials). Such a gravity + strong force approach has already been used to create attractive potential wells and quantum bound states for ultra-cold neutrons [58]. For classical dynamics the 1D cusp potential can be generated by a particle constrained to move along a suitable space curve (“frictionless bead on a wire”) falling under gravity, so long as the required forces are $< mg$. Quantum mechanically one might be able to exploit micron-scale or submicron-scale channels

as neutron guides. Polycapillary glass fibers consisting of bundles of ~ 1000 individual lead-silica glass capillaries, each with diameter $\sim 6\mu\text{m}$, have been demonstrated to act as guides for thermal neutrons [59] and are commercially available [60]. It is conjectured that neutron guides with inner diameters as small as 5-7 nm may be possible, e.g. using carbon nanotubes [61, 62]. When the diameter of the guide is comparable to the wavelength of the confined ultra-cold neutron, then simple energetic considerations as well as more detailed analysis [63, 64] imply that the wave propagation should be quasi-1D, with little excitation of high-order modes transverse to the tube axis. Using gently bent guide tubes to reduce losses [59, 63] and considering times short enough so that neutrons have velocities sufficiently small to remain confined, the 1D models of this paper might be obtained.

Another entirely different class of experiments that could realize our 1D models are based on optical analogues of Schrödinger evolution [65, 66]. For example, spatial propagation of a monochromatic light beam in guiding dielectric structures which are weakly curved along the propagation direction are described by the paraxial optical wave equation:

$$i\hbar \frac{\partial \psi}{\partial z} = -\frac{\hbar^2}{2n_s} \frac{\partial^2 \psi}{\partial x^2} + V(x)\psi - F(z)x\psi.$$

Here ψ is the complex electric field amplitude modified by reference-frame and gauge transformations, z is the paraxial propagation distance, $\hbar \equiv \lambda/2\pi$ is the reduced wavelength, $V(x) = [n_s^2 - n^2(x)]/(2n_s) \simeq n_s - n(x)$, $n(x)$ is the refractive index profile of the guiding structure, n_s is the reference (substrate) refractive index, $x_0(z)$ is the axis bending profile, and $F(z) = -n_s^2 \ddot{x}_0(z)$. For full details, see [65]. It appears feasible to produce a repulsive, cusp-like potential by manufacturing a dielectric medium with a suitable specification of $n(x) < n_s$. Such experiments are not truly quantum-mechanical, however, but are to be more properly considered as “analogue simulations” of the Schrödinger equation. Their value is to be assessed by comparison with direct numerical simulations of the Schrödinger equation, like those presented in this paper. Optical analogue experiments are useful if they can probe a complementary (or wider) range of parameters than those achievable by computer simulations.

The specific suggestions made here for experimental realization of QSS may not be the most feasible ones and, in any case, are mere sketches of possible approaches. Other possibilities will surely occur to our ingenious experimentalist colleagues. However, we believe that our theoretical analysis makes a compelling case that such breakdown of classical determinism will eventually be observed for quantum systems in the laboratory. For this not to be true, quantum mechanics itself would need to fail in the distinctive situations considered here.

VII. CONCLUSIONS

This paper has developed a novel prediction of quantum mechanics: the breakdown of determinism in the standard classical limit (large mass, small initial spreads in position and velocity) when the force-field acting on the quantum particle is nearly rough. Like the classical spontaneous stochasticity effect, it is produced by an explosive, super-ballistic acceleration of the particle and the resultant “forgetting” of its initial conditions. Quantum spontaneous stochasticity is, in some sense, a diametric opposite of Anderson localization [67]. That effect suppresses spreading of the wave-function in a random (disordered) potential, whereas QSS corresponds to an accelerated spreading. Furthermore, Anderson localization is essentially a wave-phenomenon, arising from destructive interference between multiple-scattering paths. QSS is instead an essentially classical particle phenomenon: although the origin of the randomness lies in the quantum fluctuations, quantum stochasticity is magnified to macroscopic scales by classical non-smooth dynamics.

In this paper we have confined our attention to the initial-value problem for a quantum particle, described by the non-relativistic Schrödinger equation, but QSS should appear in other guises and theoretical frameworks.

The Wigner distribution function method, previously exploited in [28], appears to be a powerful method to analyze simultaneously the position-space and momentum-space spreading of the quantum particle. There should also be very interesting manifestations of classical non-smooth dynamics in the Feynman path-integral representation of quantum scattering amplitudes [27], not only in the classical limit but also in the fully quantum-mechanical setting. Studying the quantum phenomenon will help to shed further light on classical spontaneous stochasticity, which has fundamental importance for astrophysics, geophysics, and even engineering applications. It is also critical to continue testing quantum mechanics in novel regimes that were previously unexplored.

ACKNOWLEDGMENTS

We would like to thank Eberhard Bodenschatz, Kurt Eyink, Igor Kolokolov, Jorgé Kurchan, Guy Marcus and Thomas O’Conner for very useful conversations and suggestions on possible experimental realizations of quantum spontaneous stochasticity. Abraham Harte informed us of the philosophical paper by Norton. TD would like to thank Cristian C. Lalescu and Navid Constantinou for their help with the Schrödinger simulations.

-
- [1] P. Hartman, *Ordinary Differential Equations: 2nd Ed.*, Classics in Applied Mathematics (Society for Industrial and Applied Mathematics, SIAM, 3600 Market Street, Floor 6, Philadelphia, PA 19104, 1982).
 - [2] J. Norton, *Philosopher’s Imprint* **3**, 1 (2003).
 - [3] D. Bernard, K. Gawędzki, and A. Kupiainen, *J. Stat. Phys.* **90**, 519 (1998).
 - [4] M. Chaves, K. Gawędzki, P. Horvai, A. Kupiainen, and M. Vergassola, *J. Stat. Phys.* **113**, 643 (2003).
 - [5] L. F. Richardson, *Proc. R. Soc. Lon. Ser-A* **110**, 709 (1926).
 - [6] A. Lazarian and E. T. Vishniac, *Astrophys. J.* **517**, 700 (1999).
 - [7] E. Vishniac and A. Lazarian, in *Plasma Turbulence and Energetic Particles in Astrophysics; Proceedings of the International Conference, Cracow, Poland, 5-10 September, 1999*, edited by M. Ostrowski and R. Schlickeiser (Observatorium Astronomiczne, Uniwersytet Jagielloński, Kraków, 1999) pp. 182–189.
 - [8] G. L. Eyink, A. L. Lazarian, and E. T. Vishniac, *Astrophys. J.* **743**, 51 (2011).
 - [9] G. Eyink, E. Vishniac, C. Lalescu, H. Aluie, K. Kanov, K. Bürger, R. Burns, C. Meneveau, and A. Szalay, *Nature* **497**, 466 (2013).
 - [10] G. L. Eyink, *C. R. Phys.* **7**, 449 (2006).
 - [11] G. L. Eyink, *Phys. Rev. E* **83**, 056405 (2011).
 - [12] R. Bitane, H. Homann, and J. Bec, *J. Turbul.* **14**, 23 (2013).
 - [13] M. Bourgoïn, N. T. Ouellette, H. Xu, J. Berg, and E. Bodenschatz, *Science* **311**, 835 (2006).
 - [14] A. N. Kolmogorov, *Dokl. Akad. Nauk SSSR* **30**, 299 (1941).
 - [15] L. Onsager, *Nuovo Cimento Suppl.* **6**, 279 (1949).
 - [16] G. L. Eyink and K. R. Sreenivasan, *Rev. Mod. Phys.* **78**, 87 (2006).
 - [17] B. I. Shraiman and E. D. Siggia, *Phys. Rev. E* **49**, 2912 (1994).
 - [18] G. L. Eyink and T. D. Drivas, *J. Stat. Phys.* **158**, 386 (2015).
 - [19] R. H. Kraichnan, *Phys. Fluids* **11**, 945 (1968).
 - [20] G. Falkovich, K. Gawędzki, and M. Vergassola, *Rev. Mod. Phys.* **73**, 913 (2001).
 - [21] K. Gawędzki and M. Vergassola, *Physica D* **138**, 63 (2000).
 - [22] W. E and E. Vanden-Eijnden, *Proc. Natl. Acad. Sci.* **97**, 8200 (2000).
 - [23] W. E and E. Vanden-Eijnden, *Physica D* **152-153**, 636 (2001).
 - [24] Y. L. Jan and O. Raimond, *Ann. Prob.* **30**, 826 (2002).
 - [25] Y. L. Jan and O. Raimond, *Ann. Prob.* **32**, 1247 (2004).
 - [26] T. D. Drivas and G. L. Eyink, *J. Fluid Mech.*, to be submitted.
 - [27] R. P. Feynman, *Rev. Mod. Phys.* **20**, 367 (1948).
 - [28] A. Athanassoulis and T. Paul, *Mathematical Models and Methods in Applied Sciences* **22**, 1250038 (2012).
 - [29] T. Paul, in *Microlocal Methods in Mathematical Physics and Global Analysis* (Springer, 2013) pp. 49–52.
 - [30] R. Blümel, *Acta Phys. Pol. A* **93**, 7 (1998).
 - [31] L. Couchman, E. Ott, and T. M. Antonsen Jr, *Phys. Rev. A* **46**, 6193 (1992).
 - [32] R. Blümel, T. Antonsen Jr, B. Georgeot, E. Ott, and R. Prange, *Phys. Rev. E* **53**, 3284 (1996).

- [33] See Supplemental Materials at, <http://link.aps.org/supplemental/10.1103/PhysRevX.2.041001>
- [34] M. Abramowitz and I. Stegun, *Handbook of Mathematical Functions: with Formulas, Graphs, and Mathematical Tables*, Dover Books on Mathematics (Dover Publications, 2012).
- [35] Bateman Manuscript Project, A. Erdelyi, and H. Bateman, *Higher Transcendental Functions*, vol. 1 (Dover Publications, 2007).
- [36] Bateman Manuscript Project, H. Bateman, and A. Erdélyi, *Tables of Integral Transforms: Based, in Part, on Notes Left by Harry Bateman*, v. 1 (McGraw-Hill, 1954).
- [37] R. H. Kraichnan, *Adv. Math.* **16**, 305 (1975).
- [38] A. Lazarian, E. T. Vishniac, and J. Cho, *Astrophys. J.* **603**, 180 (2004).
- [39] D. Ryu, H. Kang, J. Cho, and S. Das, *Science* **320**, 909 (2008).
- [40] A. Lazarian, *Space. Sci. Rev.* **181**, 1 (2014).
- [41] K. Gottfried and T. Yan, *Quantum Mechanics: Fundamentals*, Graduate Texts in Contemporary Physics (Springer, 2003).
- [42] L. O’Raifeartaigh and A. Wipf, *Found. Phys.* **18**, 307 (1988).
- [43] Y. Goldfarb, J. Schiff, and D. J. Tannor, *J. Chem. Phys.* **128**, 164114 (2008).
- [44] G. Barton, *Ann. Phys.* **166**, 322 (1986).
- [45] C. Yuce, A. Kilic, and A. Coruh, *Phys. Scripta* **74**, 114 (2006).
- [46] G. A. Hagedorn, *Commun. Math. Phys.* **71**, 77 (1980).
- [47] J. Vanderplas and A. Xuereb, “General numerical solver for the 1D time-dependent Schrödinger’s equation.” <https://github.com/jakevdp/pySchrodinger>, license: BSD style.
- [48] J. S. Bao, Weizhu and P. Markowich, *J. Comput. Phys.* **175**, 487 (2002).
- [49] H. Metcalf and P. van der Straten, *Laser Cooling and Trapping*, Graduate Texts in Contemporary Physics (Springer New York, 1999).
- [50] R. Grimm, M. Weidemüller, and Y. B. Ovchinnikov, *Adv. Atom. Mol. Opt. Phys.* **42**, 95 (2000).
- [51] K. Henderson, C. Ryu, C. MacCormick, and M. Boshier, *New J. Phys.* **11**, 043030 (2009).
- [52] C. Muldoon, L. Brandt, J. Dong, D. Stuart, E. Brainin, M. Himsworth, and A. Kuhn, *New J. Phys.* **14**, 073051 (2012).
- [53] H. Rauch and S. Werner, *Neutron Interferometry: Lessons in Experimental Quantum Mechanics, Wave-Particle Duality, and Entanglement*, Oxford series in neutron scattering in condensed matter (Oxford University Press, 2015).
- [54] J. Byrne, *Neutrons, Nuclei and Matter: An Exploration of the Physics of Slow Neutrons*, Dover Books on Physics (Dover Publications, 2013).
- [55] M. Utsuro and V. Ignatovich, *Handbook of Neutron Optics* (Wiley, 2010).
- [56] V. V. Vladimirkii, *Sov. Phys. JETP* **12**, 740 (1961).
- [57] T. Brenner, S. Chesnevskaya, P. Fierlinger, P. Geltenbort, E. Gutschiedl, T. Lauer, K. Rezai, J. Rothe, T. Zechlau, and R. Zou, *Phys. Lett. B* **741**, 316 (2015).
- [58] V. V. Nesvizhevsky, H. G. Börner, A. K. Petukhov, H. Abele, S. Baefler, F. J. Ruef, T. Stöferle, A. Westphal, A. M. Gagarski, G. A. Petrov, *et al.*, *Nature* **415**, 297 (2002).
- [59] H. Chen, R. G. Downing, D. F. R. Mildner, W. M. Gibson, M. A. Kumakhov, I. I. Ponomarev, and M. V. Gubarev, *Nature* **357**, 391 (1992).
- [60] R. F. Alvarez-Estrada and M. L. Calvo, in *Materials Science Forum*, Vol. 772 (Trans Tech Publ, 2014) pp. 51–56.
- [61] G. F. Calvo and R. F. Alvarez-Estrada, *Nanotech.* **15**, 1870 (2004).
- [62] S. Dabagov, *Nanosci. Nanotech. Lett.* **3**, 24 (2011).
- [63] M. L. Calvo, *J. Phys. D Appl. Phys.* **33**, 1666 (2000).
- [64] B. Rohwedder, *Phys. Rev. A* **65**, 043619 (2002).
- [65] S. Longhi, *Laser Photonics Rev.* **3**, 243 (2009).
- [66] D. Dragoman and M. Dragoman, *Quantum-Classical Analogies*, The Frontiers Collection (Springer Berlin Heidelberg, 2013).
- [67] P. W. Anderson, *Phys. Rev.* **109**, 1492 (1958).